ADDED MASS OF SUBMERGED OBJECTS OF ARBITRARY SHAPE

Ronald Betts Berklite

NAVAL POSTGRADUATE SCHOOL
Monterey, California

THESIS

ADDED MASS OF SUBMERGED OBJECTS OF ARBITRARY SHAPE

by

Ronald Betts Berklite

Thesis Advisor: C.J. Garrison

September 1972

Added Mass of Submerged Objects of Arbitrary Shape

by

Ronald Betts Berklite
Lieutenant Commander, United States Navy
A.B., Gettysburg College, 1959

Submitted in partial fulfillment of the
requirements for the degree of

MASTER OF SCIENCE IN MECHANICAL ENGINEERING

from the

NAVAL POSTGRADUATE SCHOOL
September 1972

ABSTRACT

Hydrodynamic loads induced on large underwater structures by impulsive motion may be significant design factors. Such loads may be induced by earthquake excitation or may result from acceleration produced while lifting an object in the sea.

The theoretical approach to the calculation of these loads is outlined and numerical results are presented for several submerged configurations including a vertical cone, a sphere, and a vertical circular cylinder.

Numerical results for these submerged structures are presented in the form of a dimensionless load parameter or added mass coefficient. Results corresponding to a number of different water depths are presented to show the rather sizable effect of the relative water depth on the hydrodynamic force. It is shown that the effect of the free water surface is to reduce the hydrodynamic loads in comparison to the corresponding infinite depth values.

Experimental results obtained by vibration testing are presented for a submerged sphere, a cone and a vertical cylinder. These results show excellent agreement with the theoretical results.

TABLE OF CONTENTS

LIST OF TABLES

Table Page

LIST OF FIGURES

NOMENCLATURE

Symbol Description

$\bar{a}$ = characteristic dimension of the body

A_{ij} = added mass coefficient

$\bar{d}$ = depth of submergence

$f(\xi_1,\xi_2,\xi_3)$ = source strength function

$\vec{F}$ = force vector

g = acceleration of gravity

G = Green's Function

$\bar{h}$ = depth of water

K_n = modified Bessel function of the second kind of order n

$\bar{\ell}$ = distance of line of action above bottom

$\vec{M}$ = moment vector

$\vec{n}$ = unit normal vector

p = dynamic pressure, dimensionless

P = dynamic pressure

$\vec{\bar{q}}$ = fluid velocity vector

S = surface of body

t = time

$\vec{U}$ = velocity vector of object

x_1,x_2,x_3 = coordinates, dimensionless

υ $=\sigma^2\bar{a}/g$

ξ_1,ξ_2,ξ_3 = coordinates of a point on the surface of the object, dimensionless

ρ = fluid density

Symbol	Description
σ	= frequency
ϕ	= velocity potential, dimensionless
Φ	= velocity potential
$\vec{\Omega}$	= angular vector velocity of body

ACKNOWLEDGEMENTS

The author wishes to thank Dr. C. J. Garrison of the Naval Postgraduate School, his advisor, for the suggestion of and his invaluable assistance in this study. He also gratefully thanks Kay for her encouragement and understanding.

I. INTRODUCTION

When an object is accelerated through a fluid there are, in general, two types of forces that are recognized, one being a drag component and a second, the inertial component. The nature of the flow produced by the time dependent motion of an immersed rigid object and the relative contribution of these two components of force is generally considered to be strongly dependent on the amplitude of the relative fluid motion in comparison to the characteristic lineal dimension of the object. For example, Keulegan and Carpenter [Ref. 1] found that, for harmonic motion of the fluid past a fixed circular cylinder, major flow separation did not occur and the forces were well represented by potential flow values provided the amplitude of the motion was less than about a half diameter. If the amplitude is small enough the fluid does not move in one direction far enough for separation and wake development to occur and, accordingly, an inviscid flow analysis is a valid mathematical model.

Accelerated motion of a solid body in a fluid occurs for example when a bottom mounted structure is excited by an earthquake. Other applications include the acceleration of ships and accelerated motions of objects being lifted in the ocean environment. Southerland [Ref. 2] has described the effect of added mass on the mechanics of lifting such loads as a submarine rescue chamber.

John [Ref. 3] has shown that the velocity potential associated with the harmonic motion of a rigid object immersed in a fluid with a free surface may be represented by a surface distribution of point wave sources for arbitrary values of frequency. The source distribution (or weighting) function is obtained in this formulation from the solution of an integral equation resulting from the kinematic boundary condition applied on the immersed surface. Using this technique, numerical results have been obtained, for example, for a semiellipsoid oscillating in a free surface in water of infinite depth by Kim [Ref. 4], the intended application being to surface ships. Numerical results for a bottom mounted hemisphere have been presented by Garrison and Seetharama Rao [Ref. 5] and results for several axisymmetric configurations by Milgram and Halkyard [Ref. 6]. Garrison and Chow [Ref. 7] have recently presented both theoretical and experimental results for wave forces acting on a fixed submerged oil storage tank.

In the work cited, the hydrodynamic force coefficients are represented as a function of a dimensionless frequency parameter (or equivalently, a dimensionless wave length parameter) of the form $\nu = \frac{\sigma^2 \bar{a}}{g}$ where σ denotes the frequency of the motion, $\bar{a}$ denotes the characteristic lineal dimension of the submerged object and g denotes the gravitational constant. This dimensionless parameter is essentially a form of the Froude number. In all cases, however, the

theory has a fundamental limitation. The source potential oscillates with a wave length inversely proportional to the dimensionless frequency of the motion ν, and consequently, a reasonable partition size of the immersed surface limits the validity of the numerical scheme to small to moderate values of frequency. Specifically, it has been found using the Haskind's relations [Ref. 8] and an energy balance for purposes of checking accuracy, that results can be obtained with reasonable accuracy up to about $\nu = 2.0$. Beyond this, the accuracy of the numerical results becomes questionable.

Although the range $\nu = 0$ to about 2.0 includes most applications in ship hydrodynamics and wave forces acting on large structures, the frequencies encountered, for example, in earthquake excitation corresponds to rather large values of ν in the case of large structures. Accordingly, the development of an alternate method which includes both the effect of the free surface and bottom on the hydrodynamic forces and is valid for large values of the dimensionless frequency ν is the primary objective of the present thesis. Therefore an attempt has been made herein to obtain numerical results for several different objects for the asymptotic case of very large values of ν, i.e., for the infinite Froude number case.

High frequency added mass coefficients for two-dimensional shapes oscillating on a free surface have been presented in a series of papers by Landweber et al. [Ref. 9, 10, 1,

and 12]. The motivation for this work was to provide hydrodynamic coefficients for two-dimensional ship forms.

For three-dimensional objects the only results known are those of Waugh and Ellis [Ref. 13] for the case of a sphere in infinite depth water and Jacobsen [Ref. 14] for the case of the cylindrical pier in various water depths. In the former case, the theoretical method consisted of using successive image doublets to account for the effect of the free surface. However, the case of vertical motion only was studied and their method was limited to a sphere. In the latter case, the solution was represented by a series of Bessel functions and is applicable to a vertical circular cylinder, extending between the bottom and free surface. However, the numerical computations were made using tables of Bessel functions with complex arguments which have proven misleading. In fact, Jacobsen's numerical results are in error in several instances and therefore, his analysis as well as the corrected formulae are presented herein.

In this thesis the theoretical formulation of the impulsive hydrodynamic forces acting on a rigid object of arbitrary shape is presented. The effect of the bottom and free surface is taken into consideration and the force coefficient is shown to depend on a frequency of oscillation parameter. The problem is first formulated for arbitrary values of the frequency and the asymptotic form of the solution for both large and small values of the frequency is discussed. A computer method for numerical evaluation

of the force coefficient for submerged objects of arbitrary shape is discussed and numerical results are presented for a number of specific geometric shapes including a circular cylinder, cone, and sphere. High frequency experimental results are presented for a vertical circular cylinder, sphere, and cone. These experimental results are compared with the theoretical results.

II. THEORETICAL CONSIDERATIONS

A. BOUNDARY VALUE PROBLEM

The geometry involved in the problem under consideration is shown in Figure 1. A rigid object of arbitrary shape having characteristic lineal dimension $\bar{a}$ is submerged to a depth $\bar{d}$ in water of depth $\bar{h}$ and caused to move in a small amplitude harmonic motion. The instantaneous motion of the rigid object is specified by the lineal velocity $\vec{U}$ and angular velocity $\vec{\Omega}$. The object may intersect the bottom or free surface.

Assuming an unseparated, incompressible and irrotational flow, a velocity potential $\Phi(\vec{\bar{x}},t)$ defined by

$$\vec{\bar{q}} = \vec{\nabla}\Phi \tag{1}$$

where $\vec{\bar{q}}$ denotes the fluid velocity vector, may be introduced and must satisfy the continuity equation,

$$\nabla^2\Phi = 0 \tag{2}$$

within the fluid region. The bars over the spatial variables denote dimensional quantities and $\vec{\bar{x}} = \vec{i}\bar{x}_1 + \vec{j}\bar{x}_2 + \vec{k}\bar{x}_3$.

On the rigid bottom surface described by $\bar{x}_2 = -\bar{h}$ the fluid velocity in the vertical direction must vanish and, accordingly, the corresponding kinematic boundary condition on the velocity potential is

$$\frac{\partial\Phi}{\partial\bar{x}_2}(\bar{x}_1,-\bar{h},\bar{x}_3,t) = 0 \tag{3}$$

The velocity of a point on the immersed surface is given by

$$\vec{V} = \vec{U} + \vec{\Omega} \times \vec{\bar{r}} \tag{4}$$

where $\vec{\bar{r}}$ denotes the position vector as shown in Fig. 1. The appropriate kinematic and dynamic boundary condition on the immersed surface, therefore, takes the form

$$\frac{\partial \Phi(\vec{\bar{x}},t)}{\partial \bar{n}} = \vec{V} \cdot \vec{n} \tag{5}$$

where $\vec{n} = \vec{i}n_1 + \vec{j}n_2 + \vec{k}n_3$ denotes the unit normal vector on the surface of the object and is directed outward into the fluid region.

Assuming the amplitude of the motion of the object to be small, the kinematic and dynamic boundary condition applied at the free surface may be linearized to give the well-known free surface boundary condition:

$$\frac{\partial \Phi}{\partial \bar{x}_2}(\bar{x}_1,0,\bar{x}_3,t) + \frac{1}{g}\,\frac{\partial^2 \Phi(\bar{x}_1,0,\bar{x}_3,t)}{\partial t^2} = 0 \tag{6}$$

Furthermore, if the object oscillates with frequency σ, the time dependence of the velocity potential may be separated and written as $\mathrm{Re}[\phi(\bar{x}_1,\bar{x}_2,\bar{x}_3)e^{-i\sigma t}]$ where Re denotes the real part. In which case Eq. (6) becomes

$$\frac{\partial \phi}{\partial x_2}(x_1,0,x_3) - \frac{\sigma^2 \bar{a}}{g}\,\phi(x_1,0,x_3) = 0 \tag{7}$$

where the unbarred quantities represent the coordinates made dimensionless with $\bar{a}$.

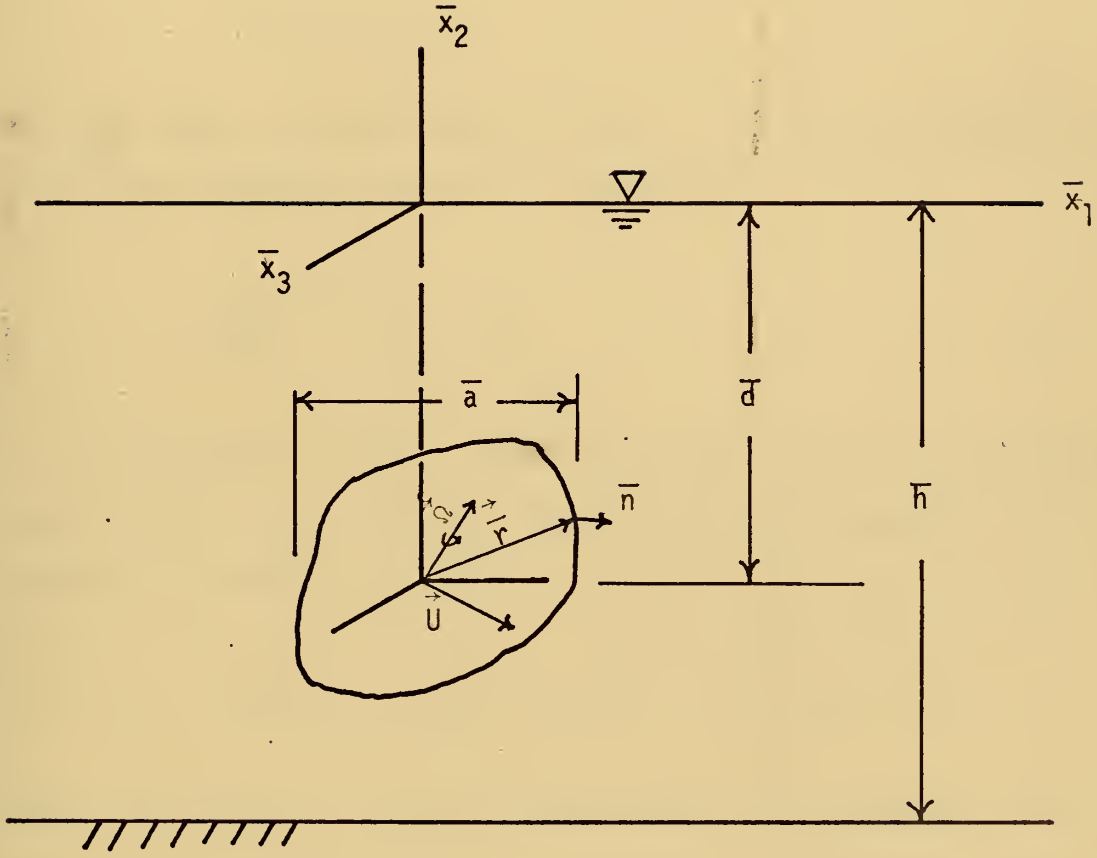

Fig. 1 - Definition of Geometry

In general it is apparent from Eq. (7) that the solution to the boundary value problem established must depend on the dimensionless frequency parameter $\sigma^2\bar{a}/g$. However, there are two extreme cases where the results become independent of the frequency. These correspond to the case where $\sigma^2\bar{a}/g \to \infty$ in which case Eq. (7) becomes

$$\phi(x_1,0,x_3) = 0 \quad . \qquad (8)$$

For the other extreme where $\sigma^2\bar{a}/g \to 0$ the free surface appears as a rigid boundary as Eq. (7) becomes

$$\frac{\partial\phi}{\partial x_2}(x_1,0,x_3) = 0 \qquad (9)$$

If consideration is restricted to either of the boundary conditions Eq. (8) or Eq. (9) the velocity potential may be written as the sum

$$\phi(\vec{\bar{x}},t) = W_i(t)\ \phi_i(\vec{\bar{x}}), \qquad i = 1,2,\ldots 6 \qquad (10)$$

where each term in the sum represents the potential associated with the i^{th} component of body motion. ($i = 1,2,3$ refers to linear motion components in the $\bar{x}_1,\bar{x}_2,\bar{x}_3$ directions, respectively, and $i = 4,5,6$ refers to the angular motion components about the $\bar{x}_1,\bar{x}_2,\bar{x}_3$ axes, respectively.) The time dependent function W is defined as

$$\left.\begin{aligned} W_i(t) &= U_i(t)\ \bar{a} \\ W_{i+3}(t) &= \Omega_i(t)\ \bar{a}^2 \end{aligned}\right\} \quad i = 1,2,3 \qquad (11)$$

in which the symbols U_i and Ω_i denote the components of the lineal and angular velocity vectors of the body, $\vec{U}$ and $\vec{\Omega}$, respectively. The potentials ϕ_i are dimensionless quantities.

It is important to note that the application of either of the two boundary conditions, Eqs. (8) and (9), makes the problem homogeneous in time. Consequently, the assumption of harmonic motion may be relaxed and the functions $W_i(t)$ may be allowed to be arbitrary functions.

Substituting Eq. (10) into Eqs. (2), (3), (5) and (8) or (9) and introducing the dimensionless variables defined as

$$x_i = \bar{x}_i/\bar{a}, \quad h = \bar{h}/\bar{a}, \quad d = \bar{d}/\bar{a} \tag{12}$$

the boundary value problem for ϕ_i $(i = 1,2,\ldots 6)$ may be specified as follows:

$$\begin{aligned}
&\nabla^2\phi_i(x_1,x_2,x_3) = 0\\
&\phi_i(x_1,0,x_3) = 0, \ (\sigma\to\infty) \quad \text{or} \quad \frac{\partial\phi_i}{\partial x_2}(x_1,0,x_3) = 0, \ (\sigma\to 0)\\
&\frac{\partial\phi_i(x_1,-h,x_3)}{\partial x_2} = 0\\
&\frac{\partial\phi_i(x_1,x_2,x_3)}{\partial n} = m_i \quad \text{(on the immersed surface)}
\end{aligned} \tag{13 a-d}$$

where

$$\begin{aligned}
m_i &= n_i \ , \ i = 1,2,3\\
m_4 &= (x_2+d)n_3 - x_3n_2\\
m_5 &= x_3n_1 - x_1n_3\\
m_6 &= x_1n_2 - (x_2 + d)n_1
\end{aligned} \tag{14 a-d}$$

The boundary conditions (13b) represent two different possibilities on the free surface, the first being the high frequency condition and the second the rigid boundary (or zero frequency) condition. In as much as the method of solution involving either boundary condition is similar, both solutions are developed simultaneously in the following.

B. GREEN'S FUNCTION SOLUTION

The solution to the boundary value problem (13) may be carried out by use of a Green's function. The Green's function represents the potential for a point source and these sources are distributed over the immersed surface according to the distribution function $f(\vec{\xi})$. According to this concept the potential ϕ may be written as

$$\phi_i(\vec{x}) = \frac{1}{4\pi} \int\int_S f_i(\vec{\xi})\, G(\vec{x};\vec{\xi})dS \tag{15}$$

where $(\vec{\xi})$ denotes a point on the immersed surface, G denotes the Green's function and $dS = d\bar{S}/\bar{a}^2$ denotes the surface area element made dimensionless with the characteristic body dimension $\bar{a}$.

In order that Eq. (15) represent a solution to Eqs. (13) it is necessary that G satisfy the equation

$$\nabla^2 G(\vec{x};\vec{\xi}) = \delta(\vec{x}-\vec{\xi}) \tag{16}$$

where $\delta(x)$ denotes the Dirac delta function, as well as boundary conditions (13c) and (13b).

The Green's function satisfying Eq. (16) as well as Eq. (13b) and (13c) is obtained by use of successive images of sources as depicted in Fig. 2 and is given by

$$G(\vec{x};\vec{\xi}) = \frac{1}{R} - \frac{1}{R_1} + \sum_{n=1}^{\infty} \left[(-1)^n \left(\frac{1}{R_{2_n}} + \frac{1}{R_{4_n}}\right) + (-1)^{n+1}\left(\frac{1}{R_{3_n}} + \frac{1}{R_{5_n}}\right)\right] \tag{17}$$

The corresponding form of G satisfying the rigid boundary condition Eq. (13c) ($\sigma = 0$ on $x_2 = 0$) is also obtained by successive images and is similar to Eq. (17) except that all of the sources have positive strengths. For this case, the Green's function takes the form

$$G(\vec{x};\vec{\xi}) = \frac{1}{R} + \frac{1}{R_1} + \sum_{n=1}^{\infty} \left(\frac{1}{R_{2_n}} + \frac{1}{R_{3_n}} + \frac{1}{R_{4_n}} + \frac{1}{R_{5_n}}\right) \tag{18}$$

where in both Eq. (17) and (18)

$$\begin{aligned}
\omega &= \sqrt{(x_1 - \xi_1)^2 + (x_3 - \xi_3)^2} \\
R &= \sqrt{\omega^2 + (x_2 - \xi_2)^2} \\
R_1 &= \sqrt{\omega^2 + (x_2 + \xi_2)^2} \\
R_{2_n} &= \sqrt{\omega^2 + (x_2 - 2nh - \xi_2)^2} \\
R_{3_n} &= \sqrt{\omega^2 + (x_2 + 2nh + \xi_2)^2}
\end{aligned} \tag{19}$$

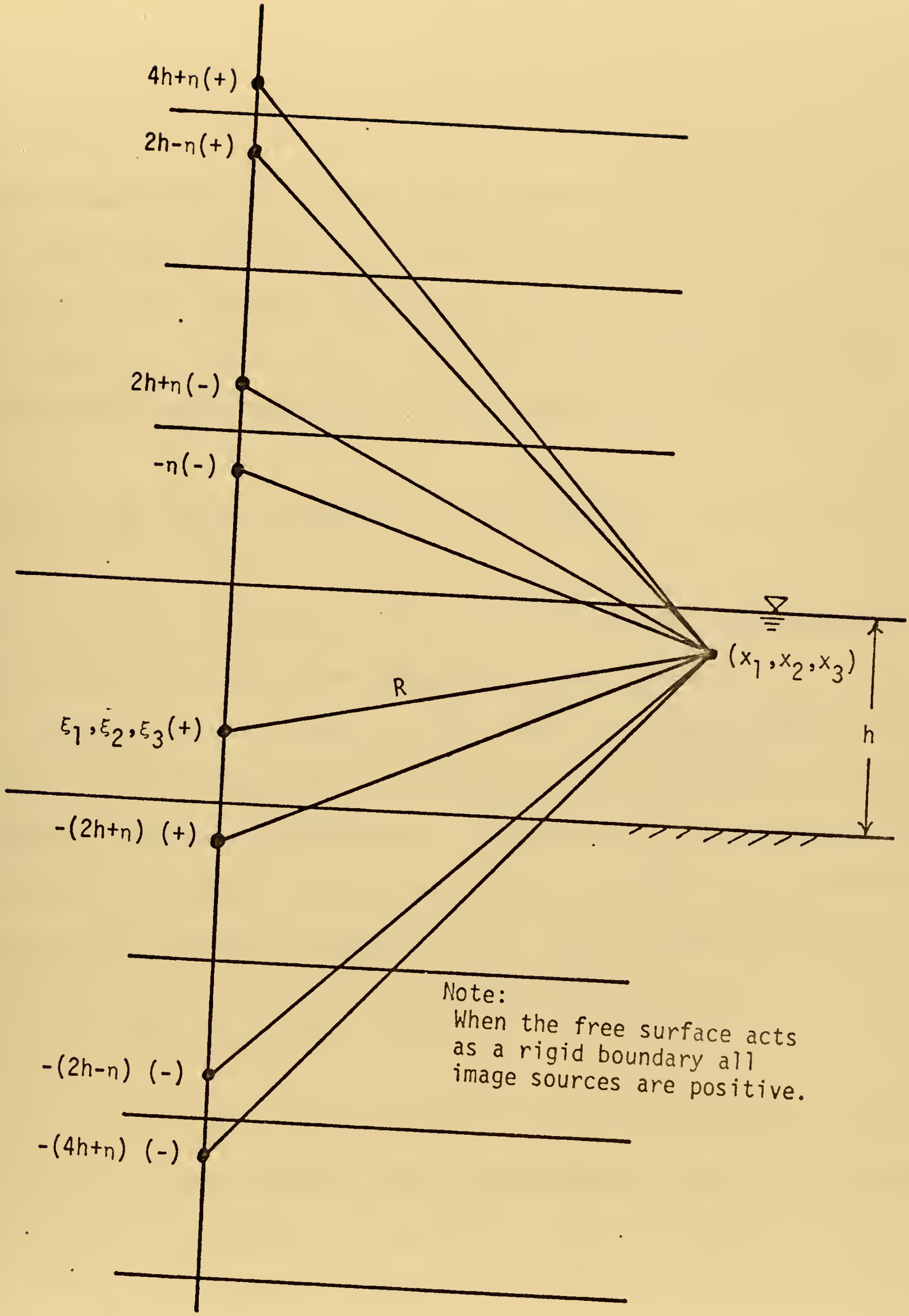

Note:
When the free surface acts as a rigid boundary all image sources are positive.

Fig. 2 - Image source layout.

$$R_{4_n} = \sqrt{\omega^2 + (x_2 + 2nh - \xi_2)^2}$$

$$R_{5_n} = \sqrt{\omega^2 + (x_2 - 2nh + \xi_2)^2}$$

Since G satisfies Eq. (13a-d) the potential ϕ_i as given by Eq. (15) must also satisfy these conditions. Thus, it remains to select the function f such that Eq. (13d) is satisfied. Application of this boundary condition yields the following Fredholm integral equation of the second kind

$$-f_i(\vec{x}) + \frac{1}{2\pi} \iint_S f_i(\vec{\xi}) \frac{\partial G(\vec{x};\vec{\xi})}{\partial n} \, dS = 2m_i(\vec{x}) \quad , \ i = 1,2,\ldots 6 \qquad (20)$$

which is to be solved for $f(\vec{\xi})$. This integral equation is to be satisfied at all points $\vec{x}$ on the immersed surface.

Because of the form of G, Eq. (20) is rather complex and it is therefore necessary to carry out the solution to the integral equation numerically. Proceeding in this direction the immersed surface may be partitioned into N area elements of size ΔS_i and the integral in Eq. (20) written as the sum

$$-f_{n_i} + f_{n_j} \alpha_{ij} = 2m_{n_i} \quad , \qquad n = 1,2,\ldots 6 \qquad (21)$$

where i,j = 1,2,...N and n refers to the six possible modes of motion of the object. The transformation from the integral equation to a summation is possible since f is a well-behaved function. It follows from Eq. (20) that the coefficient matrix is defined by

$$\alpha_{ij} = \frac{1}{2\pi} \int\int_{\Delta S_j} \frac{\partial G(\vec{x}_i;\vec{\xi})}{\partial n} \, dS \tag{22}$$

The function $\partial G/\partial n$ in Eq. (22) is obtained in a straightforward manner by differentiation of Eq. (17) or (18).

Once the coefficient matrix α_{ij} is obtained from Eq. (22) a standard digital computer subroutine may be used to invert the matrix equation, Eq. (21), to obtain the source strength f at points on the immersed surface. For purposes of evaluation of G and $\partial G/\partial n$ by use of (17) and (18) it was found that about 15 terms were adequate. The data presented herein, however, were obtained using 30 terms.

C. HYDRODYNAMIC FORCES AND MOMENTS

The dynamic fluid pressure is obtained from the linearized form of Bernoulli's equation as

$$P = -\rho \frac{\partial \Phi}{\partial t} \tag{23}$$

where the velocity squared term has been neglected. Corresponding to the i^{th} component of body motion, the pressure is obtained by use of Eq. (10) and (23) as

$$P_i = -\rho \dot{w}_i \phi_i \text{ (no sum)} \qquad i = 1,2,\ldots 6 \tag{24}$$

The pressure may further be written in dimensionless coefficient form as

$$p_i(\vec{x}) = \frac{P_i(\vec{x})}{\rho \dot{w}_i} = -\phi_i(\vec{x}) , \qquad i = 1,2,\ldots 6 \tag{25}$$

The hydrodynamic force acting on the object is obtained by carrying out the integration of the pressure over the immersed surface. Using Eq. (24) the force vector associated with the j^{th} component of body motion is

$$\vec{F}_j = -\bar{a}^2 \iint_S P_j \vec{n} dS, \qquad j = 1,2,\ldots 6 \qquad (26)$$

The corresponding result for the moment vector is

$$\vec{M}_j = -\bar{a}^3 \iint_S P_j \; \vec{r} \times \vec{n} \; dS, \qquad j = 1,2,\ldots 6 \qquad (27)$$

Using Eq. (24) as well as the definition of m_i as given in Eq. (14), the i^{th} component of force associated with the j^{th} component of acceleration is given in dimensionless coefficient form as

$$A_{ij} = \frac{F_{ij}}{\rho \bar{a}^2 \dot{w}_j} \iint_S \phi_j m_i \; dS, \qquad \begin{array}{l} i = 1,2,3 \\ j = 1,2,\ldots 6 \end{array} \qquad (28)$$

and the corresponding expression for moment is

$$A_{ij} = \frac{M_{ij}}{\rho \bar{a}^3 \dot{w}_j} \iint_S \phi_j m_i \; dS, \qquad \begin{array}{l} i = 4,5,6 \\ j = 1,2,\ldots 6 \end{array} \qquad (29)$$

where w is defined by Eq. (11).

Equations (28) and (29) define the inertia (or added mass) tensor having, in general, 36 elements. The dimensionless coefficients A_{ij} defined by Eq. (28) represent the dimensionless force coefficient and Eq. (29) represents the dimensionless moment coefficient. These coefficients are generally referred to as added mass (or moment of inertia) coefficients.

Although these coefficients are made dimensionless by use of $\bar{a}$ in the definitions (28) and (29), there are cases, depending on the body geometry, where other length scales are more appropriate. It is also standard practice in many cases to use the displaced fluid volume. However, in all numerical results presented herein the definition of A_{ij} is specified on the figure so that although the definitions vary, no confusion should result.

For purposes of numerical evaluation of the coefficients given in Eqs. (28) and (29) the integrals may be written as the summation, where the integral sign has been replaced by the sum on the k index.

$$A_{ij} = (\phi_j m_i)_k \, \Delta S_k \quad , \qquad \begin{matrix} i,j = 1,2,\ldots 6 \\ k = 1,2,\ldots N \end{matrix} \tag{30}$$

However, in order to apply Eq. (30) it is necessary to first evaluate ϕ_j at all of the nodal points on the immersed surface. For this purpose the surface integration in Eq. (15) is also converted to the summation

$$(\phi_j)_k = \beta_{k\ell} (f_j)_\ell \quad , \qquad \begin{matrix} j = 1,2,\ldots 6 \\ k,\ell = 1,2,\ldots N \end{matrix} \tag{31}$$

where the coefficient matrix is defined as

$$\beta_{k\ell} = \frac{1}{4\pi} \iint_{\Delta S_\ell} G(\vec{x}_k ; \vec{\xi}) \quad dS \tag{32}$$

Once the coefficient matrix is evaluated by Eq. (32), the summation indicated in Eq. (31) may be carried out

determine ϕ_j at all nodal points on the immersed surface. The coefficients A_{ij} are then obtained by use of Eq. (30).

Although there are 36 possible added mass coefficients defined by Eqs. (28) and (29), many are zero on account of symmetry and most off-diagonal elements are small. Also, even for a body of arbitrary shape A_{ij} is symmetrical so that at most only 21 of the coefficients need be evaluated. That is, Eq. (13$\overset{d}{\text{e}}$) along with Eq. (28) and (29) gives

$$A_{ij} = \iint_S \phi_j m_i \, dS = \iint_S \phi_j \frac{\partial \phi_i}{\partial n} \, dS \tag{33}$$

By use of the Green's theorem applied to the fluid region external to the body, it can be shown that

$$\iint_S \phi_j \frac{\partial \phi_i}{\partial n} \, dS = \iint_S \phi_i \frac{\partial \phi_j}{\partial n} \, dS \tag{34}$$

since on the free surface either $\phi = 0$ or $\partial\phi/\partial n = 0$ (depending on the boundary condition being enforced) and $\partial\phi/\partial n = 0$ on the bottom. Therefore, in view of Eq. (34) and (33) it is apparent that the added mass tensor is symmetrical,

$$A_{ij} = A_{ji} \tag{35}$$

D. JACOBSEN'S SOLUTION

At this juncture it is appropriate to comment on the analytical solution presented by Jacobsen [Ref. 2] for the special case of a vertical circular cylinder extending between

a rigid bottom and a free surface. This solution represents the only known analytical result for the problem under consideration and, therefore, is of considerable value as a point of comparison for the numerical results presented herein. However, it was found that a number of errors were present in Jacobsen's work and it was necessary to re-develop and re-evaluate the equations. The expression for the added mass coefficient associated with horizontal acceleration in terms of the notation of the present paper and in terms of Bessel functions having real as opposed to imaginary arguments appears as

$$A_{11} = \frac{16h}{\pi^3} \sum_{n=1,3,5} \frac{1}{n} B_n K_1\left(\frac{n\pi}{2h}\right) \tag{36}$$

where A_{11} denotes the added mass coefficient made dimensionless with the displaced volume, the factor B_n is defined as

$$B_n = \frac{1/n^2}{K_o\left(\frac{n\pi}{2h}\right) + \frac{2h}{n\pi} K_1 \left(\frac{n\pi}{2h}\right)} \tag{37}$$

and K_o and K_1 denote modified Bessel functions of the second kind of order zero and one, respectively. This expression agrees with Jacobsen's corresponding expression with the exception of a factor of 2.0 and the type of Bessel functions involved. It was found that more serious sign errors occurred in Jacobsen's expression for the line of action of the horizontal hydrodynamic force and, accordingly, his numerical

results are also in error. The correct expression for the elevation of the line of action (or center of added mass) in terms of the notation of the present paper is

$$\ell = \frac{\displaystyle\sum_{n=1,3,5} \frac{1}{n}\left[1+(-1)^{\frac{n+1}{2}} \frac{2}{n\pi}\right] B_n K_1\left(\frac{n\pi}{2h}\right)}{\displaystyle\sum_{n=1,3,5} \frac{1}{n} B_n K_1\left(\frac{n\pi}{2h}\right)} \tag{38}$$

where $\ell = \bar{\ell}/\bar{h}$, $\bar{\ell}$ being the elevation of the line of action above the bottom and $\bar{h}$ the water depth.

For completeness the expression for the dimensionless pressure on the surface of the cylinder is given in terms of the notation of the present paper as

$$p = -\frac{8h}{\pi^2} \cos\theta \sum_{n=1,3,5} (-1)^{\frac{n+1}{2}} \cos\left[\frac{n\pi}{2h}(h+y)\right] B_n K_1\left(\frac{n\pi}{2h}\right) \tag{39}$$

where θ denotes the angle measured with respect to the x-axis in the x-z plane.

Equations (36) and (37) were programmed for numerical evaluation on a digital computer so that an adequate number of terms could be evaluated without concern over numerical error. These results are plotted in Figs. 8 and 9 for comparison with the source distribution results developed

herein. It was noted that numerical results obtained from figures presented by Jacobsen [Ref. 2] are in error when compared to numerical results obtained from Eqs. (36) and (38).

III. EXPERIMENTAL APPROACH

Experiments were conducted to determine the added mass coefficient of a circular cylinder, a cone and a sphere in proximity of a free surface and rigid bottom. The basic experimental approach consisted of mounting the test object on flexible beams and measuring its natural frequency of vibration in air and water. The reduction in natural frequency when placed in water was then related to the added mass of the water.

The test rig was used to determine the added mass coefficient corresponding to the horizontal motion is shown in Fig. 3 and 4. The sphere was mounted in this test rig on a thin 6 inch long by 2 inch chord vertical strut. Two large steel channels were placed perpendicular to each other and welded to a 1/2-inch steel plate to form a rigid support for the spring-mass system. These channels were supported at four points on the top edge of a shallow, water-tight box (24" x 70" x 48"). The cylinder, cone, and sphere, mounted on a pair of flexible beams, were bolted to this supporting structure as shown in Fig. 3. (The cylinder is shown.)

Four strain gages were mounted on the upper end of one of the flexible beams and connected into a Wheatstone bridge. The bridge was then connected to a carrier pre-amplifier and the frequency of the bridge output was measured

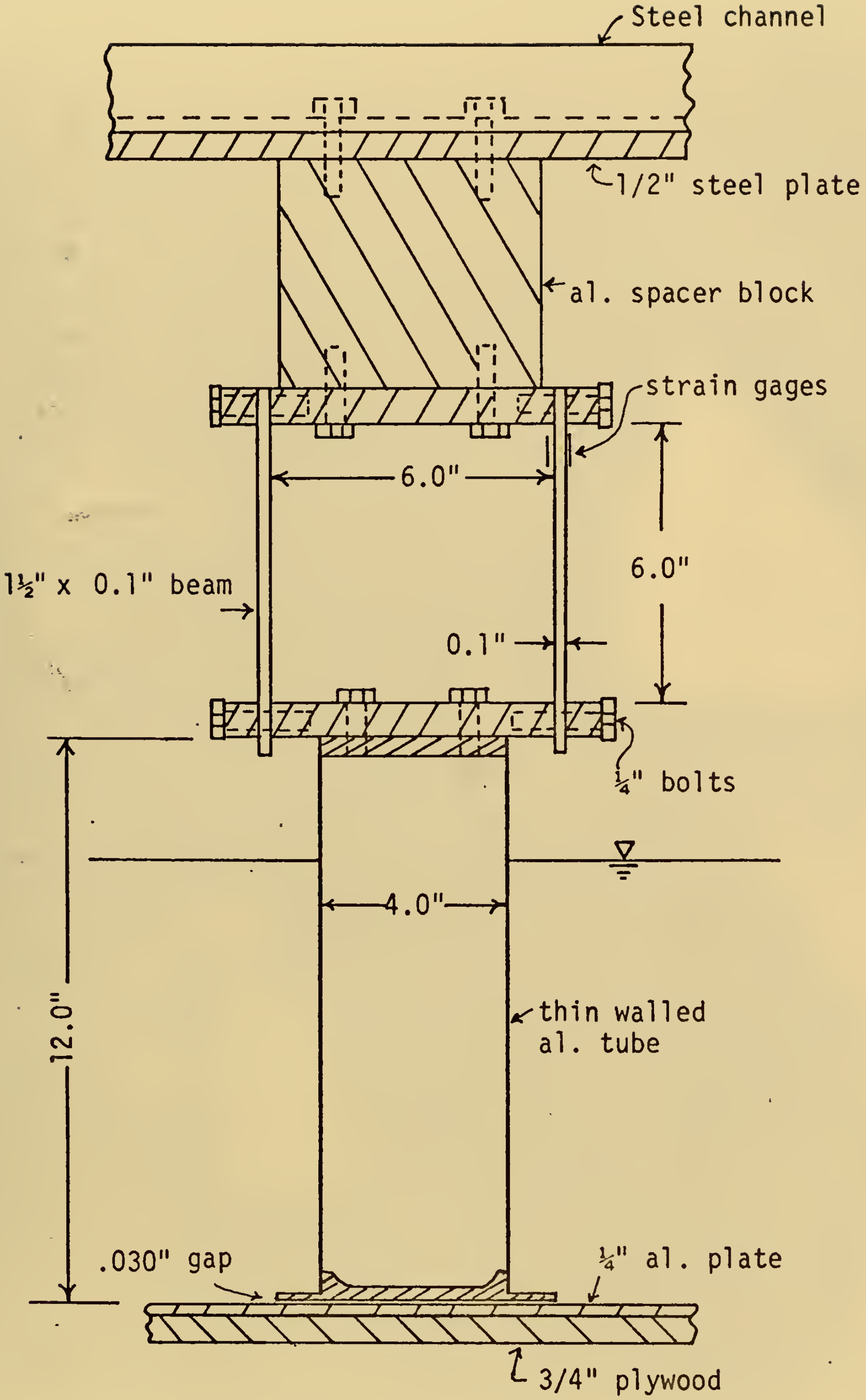

Fig. 3 - Experimental equipment.

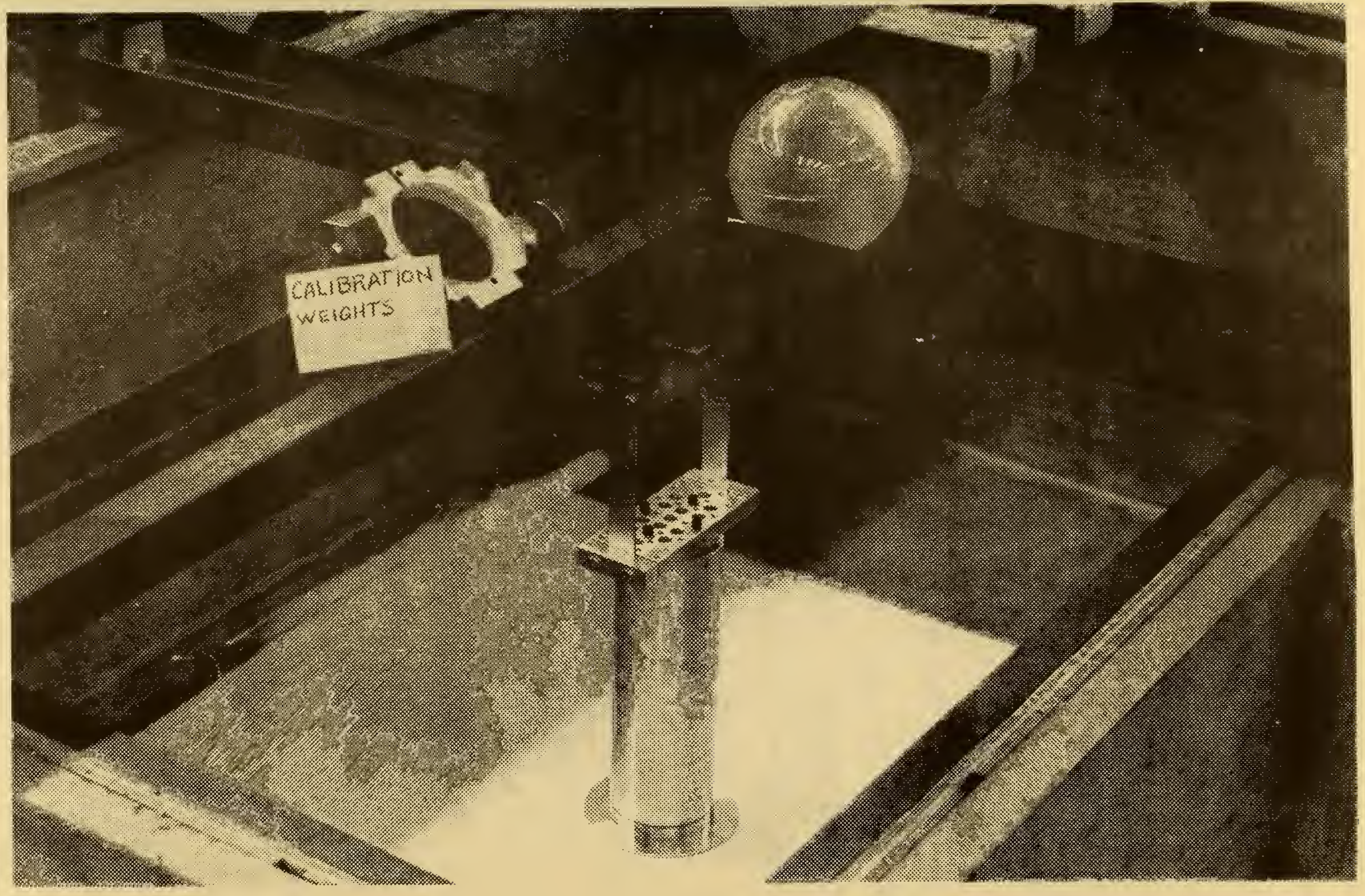

Fig. 4 - Experimental apparatus.

by use of a Monsanto programmable counter-timer and in some cases by the use of a Visicorder. A ten second duration was set on the counter-timer and, depending on the depth of water and test object, the readings ranged from about 110 to 180 cycles. The time duration programmed on the counter was highly accurate so that the major error in the process was considered to result from reading the number of cycles occurring in the 10 second interval to integer values. However, since the starting of the interval was random, this error was minimized by repeating each test run six times and recording the average reading. It was noted that the spread in readings from the counter was never greater than one cycle in the ten second interval for a given configuration.

A calibration curve for the system was developed by plucking the mass (test object) in the air with the addition of pre-measured weights attached to the test object. As a result it was unnecessary to rely on the theoretical natural frequency equation for the spring-mass system. In general, the test procedure was considered to be highly accurate and good repeatability was obtained in all cases. The calibration curves are shown in Appendix C.

The same procedure was used for the determination of the added mass coefficients for the sphere in vertical motion but a different apparatus and tank was employed. The parallel beam mount which carried the rod with attached

inch diameter plexiglass sphere is shown in Fig. 5 and 6. The tank used in this experiment was 4.0 ft. deep and represented, for practical purposes, an infinite depth case. The sphere was oscillated in the vertical direction.

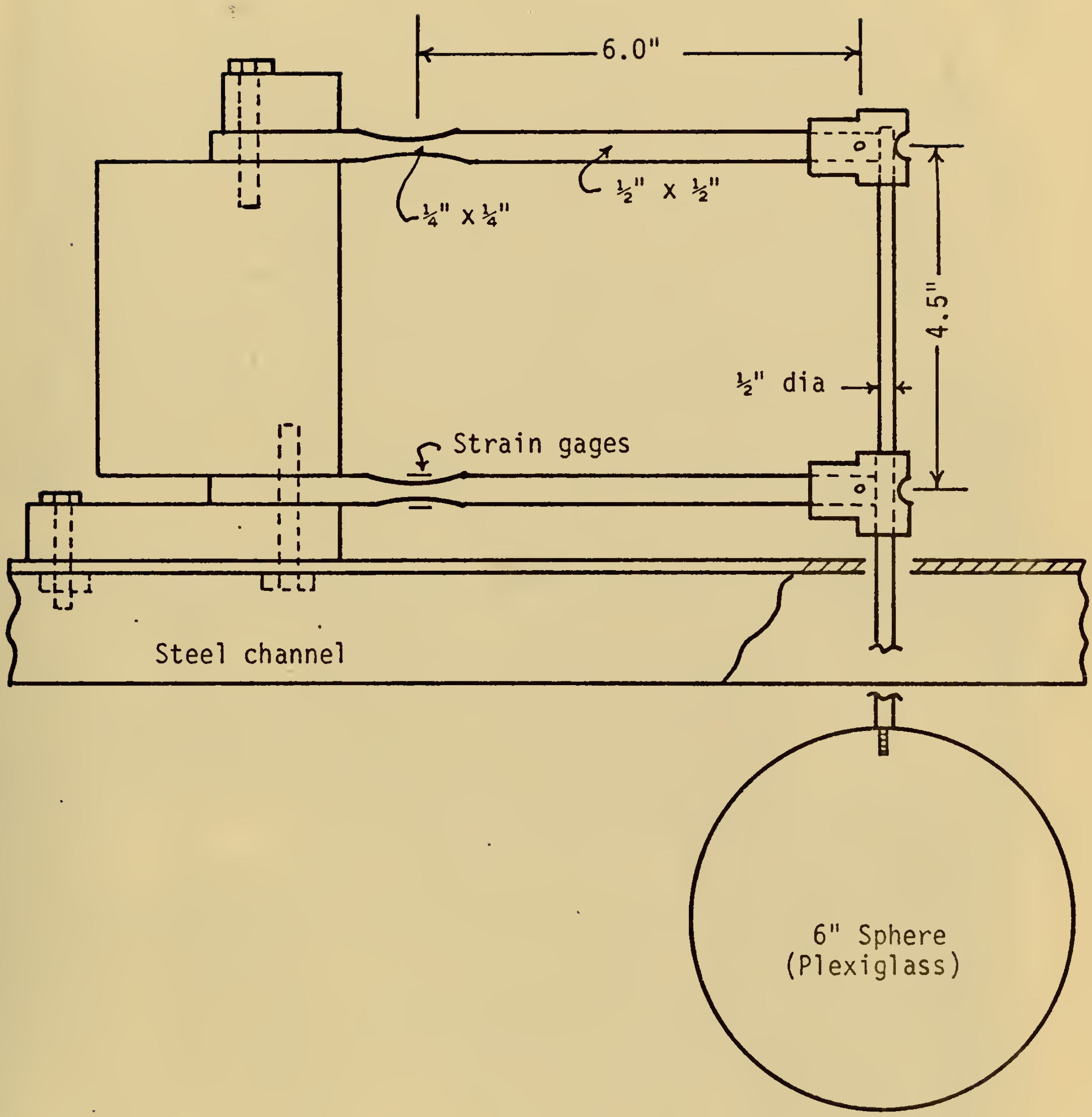

Fig. 5 - Experimental apparatus used in heave tests.

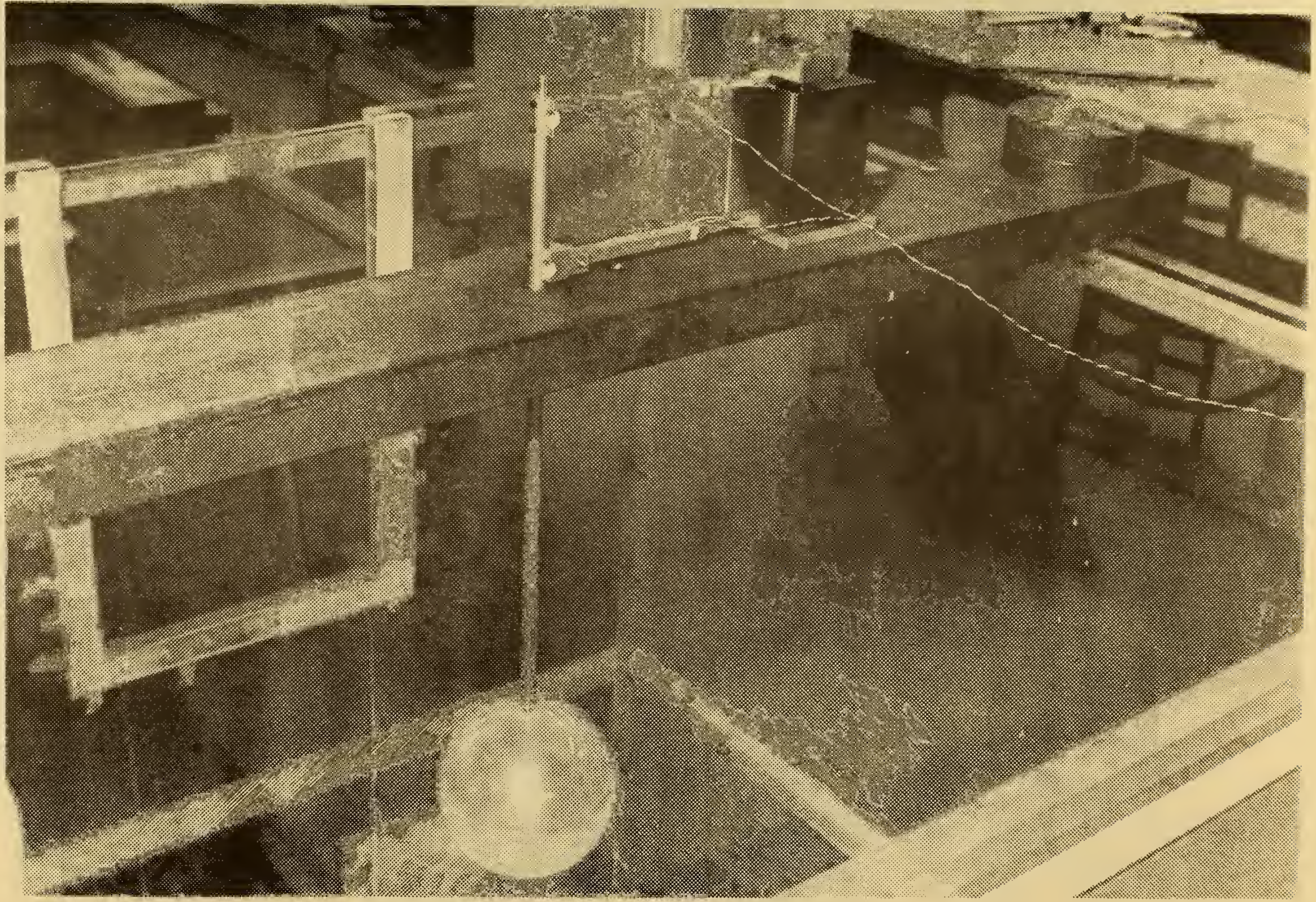

Fig. 6 - Experimental apparatus.

IV. DISCUSSION OF RESULTS

A. CIRCULAR CYLINDER

Theoretical and experimental values of added mass coefficients have been generated for a number of configurations and are plotted in Figs. 7-20 and tabulated in Tables 1-18. These include results for a vertical circular cylinder, a sphere, a hemispherical bottom-mounted vessel, and a conically-shaped object.

The theoretical and experimental results for the added mass coefficient for a vertical circular cylinder are shown in Figs. 7-12 and Tables 1-7. The calibration curves are presented in Fig. 7. Two different cylinders of the same overall dimensions and materials were used. They produced calibration curves which were slightly different results since their natural frequencies of vibration were different and their positions in the test rig could not be duplicated exactly.

The added mass coefficient corresponding to the case of the horizontal acceleration as based on the cylinder radius cubed is presented in Fig. 8, both with a free surface and with a rigid upper boundary. Results for two different grid sizes are shown, 120 and 192 effective nodal points, and little difference was found to exist. It can be seen that the computer results for the "rigid boundary" case closely follow the straight line relationship (πh) representing the classical two-dimensional result. The

results corresponding to the "free surface" case show that the effect of the free surface is to reduce the added mass coefficient and for larger values of h the results appear to be closely approximated by the straight line relationship $A_{11} = (\pi h - 3.0)$.

The same type of result in a slightly different form is presented in Fig. 9. In this figure the added mass coefficient made dimensionless in the more common manner, by use of the displace volume $\pi \bar{a}^2 \bar{h}$, is plotted for two different grid sizes along with Jacobsen's results, Eq. (36). Also, the experimental results obtained from vibration testing are presented for comparison.

The results show that the effect of the free surface is to reduce the added mass coefficients and agreement between the experimental and theoretical results is shown to be excellent. On the same figure the computer results for the rigid boundary case are presented. The classical result for two-dimensional flow gives $A_{11} = 1.0$ and, therefore, the deviation from this value gives the percentage numerical error in the computer results directly. The figure indicates a maximum of about 3.0 per cent error at the extreme low values of h.

There is no doubt that accuracy of the computer results could be improved by means other than the most obvious: increasing the number of area elements. However, any gain in precision is generally offset by increased computer storage requirements, complexity and computer run time. The

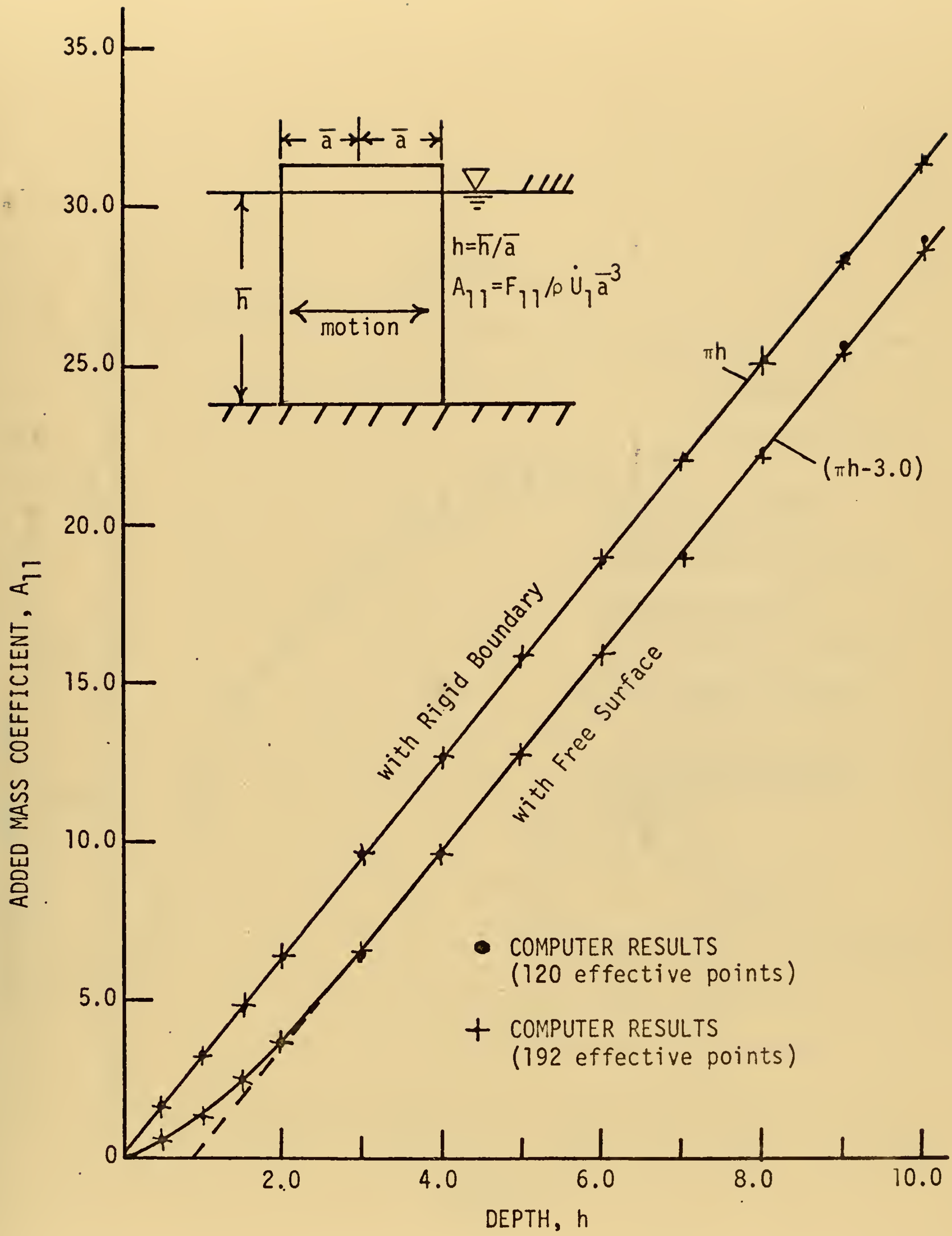

Fig. 8 - Added mass coefficient for a vertical circular cylinder.

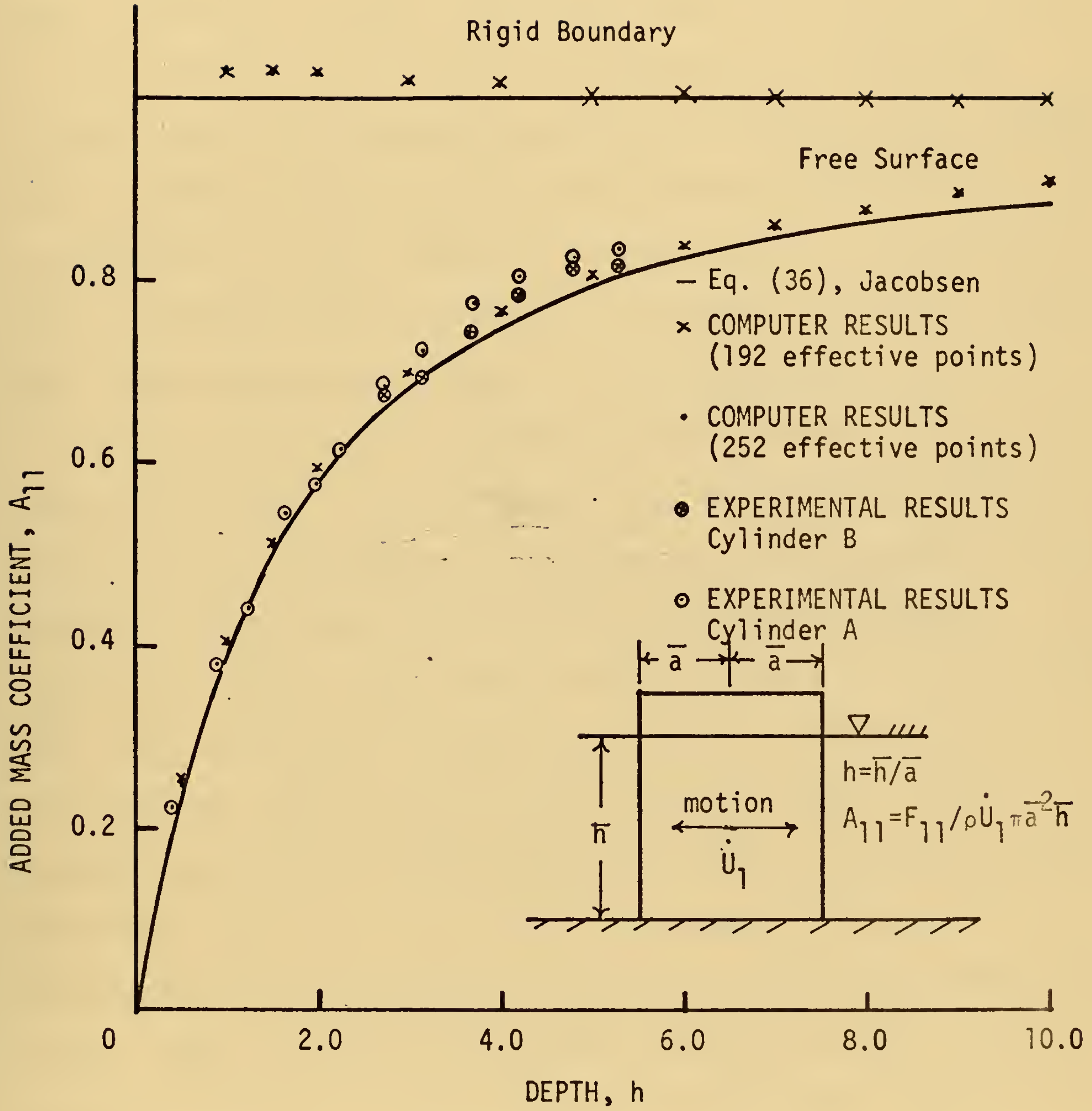

Fig. 9 - Added mass coefficient for a vertical circular cylinder.

present method is considered to be quite simple and versatile with respect to configuration and yet possesses adequate accuracy for most purposes.

For the case of horizontal motion, the line of action of the horizontal force is also a parameter of interest. When the upper boundary acts as a "wall", the force acts at the center, i.e., at ℓ = .5. However, for the free surface case the pressures are reduced near the free surface and the line of action is somewhat below center. This result is presented in Fig. 10 as obtained using 252 nodal points and is compared with Jacobsen's corrected result, Eq. (38). The figure shows the agreement to be excellent.

A second degree of freedom is also possible for the vertical cylinder. The cylinder may be allowed to rotate about some convenient axis with angular acceleration. In which case an added moment of inertia may be defined. Numerical results have been generated, using 192 nodal points, for this coefficient for rotation about an axis passing through the center of the cylinder at its base. These theoretical results are presented in Fig. 11. The results show that the free surface has the effect of reducing the hydrodynamic reaction when compared to the rigid boundary case. This is the expected result since the free surface tends to reduce the pressure differential near the top of the cylinder.

Finally, in order to show how the maximum pressure on the surface of the cylinder varies with depth, Fig. 12 as

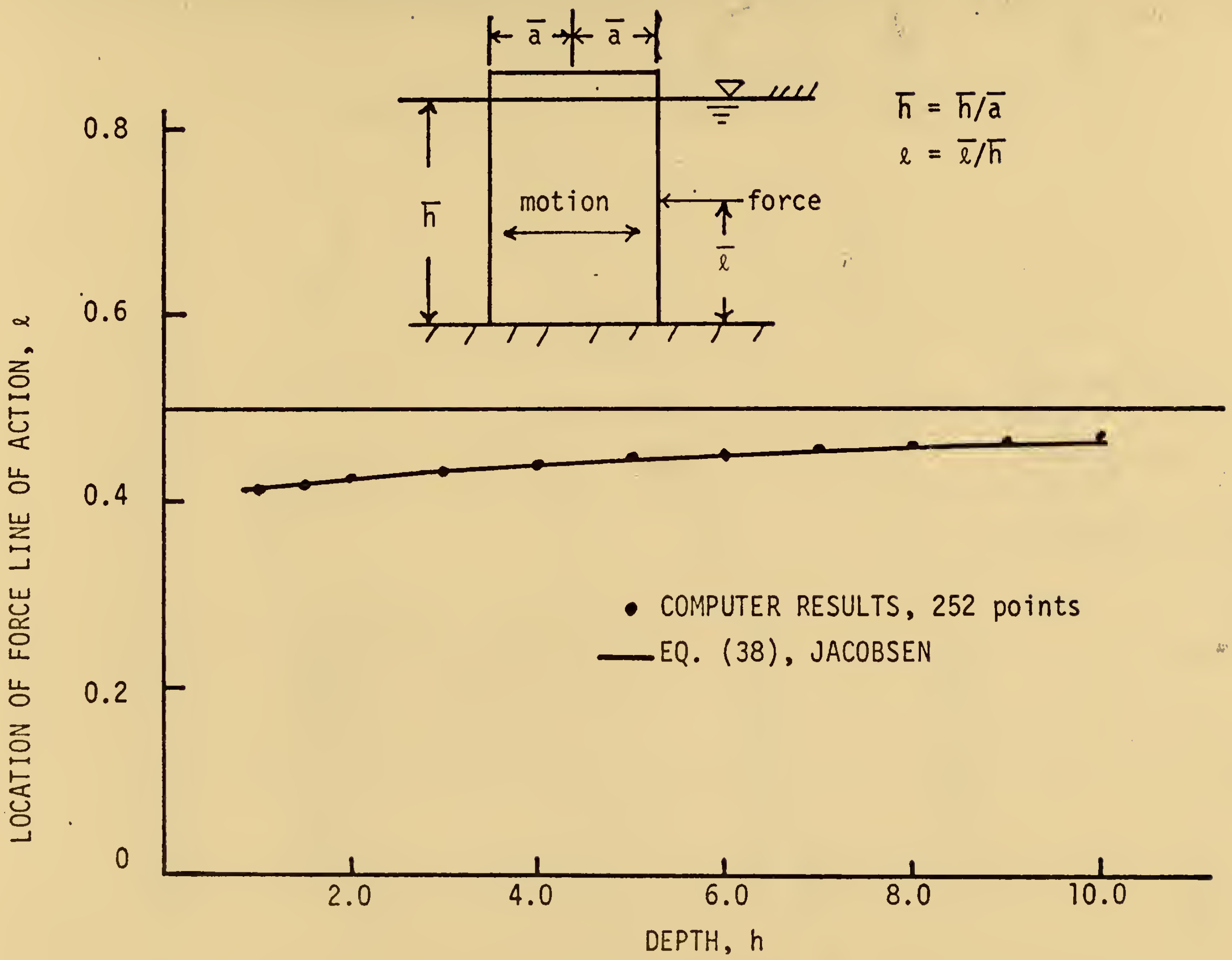

Fig. 10 - Location of effective line of action of hydrodynamic inertia force for a vertical circular cylinder.

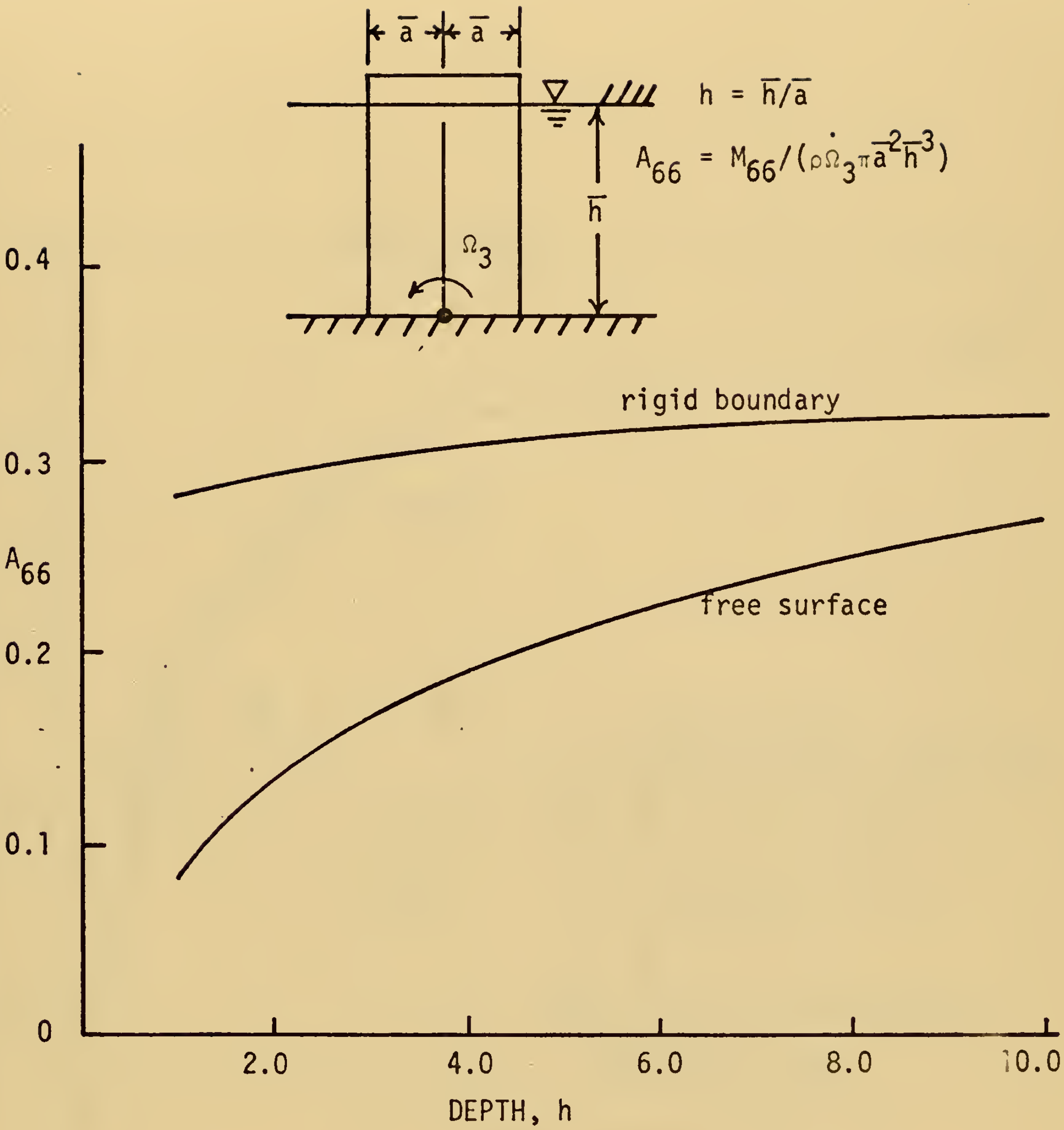

Fig. 11 - Added moment of inertia coefficient for a vertical circular cylinder.

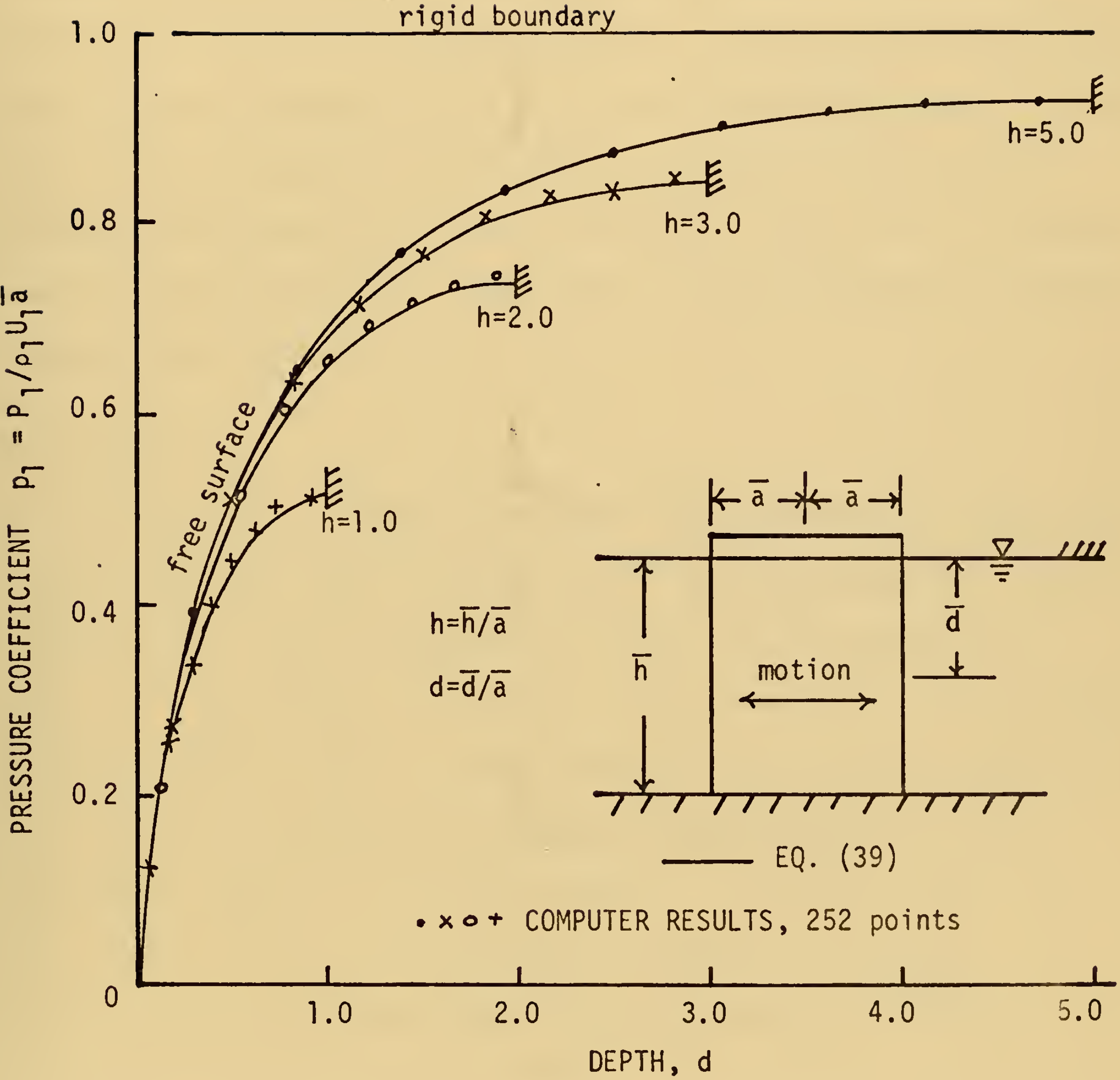

Fig. 12 - Pressure amplitude on meridian of a vertical cylinder.

been prepared. In this figure the dimensionless pressure coefficient as defined by Eq. (25) is plotted for the case of horizontal acceleration. It may be noted that the classical solution corresponding to the rigid boundary case yields the maximum pressure of $p_1 = 1.0$ over the complete length. Fig. 11 shows that the pressure corresponding to the free surface case begins at zero and appears to approach unity as the distance from the free surface and depth increase. This is the expected trend since the effect of the free surface diminishes at large distances. Eq. (39) is plotted on the same figure for comparison and the agreement appears to be quite good.

B. SPHERE

Results for a sphere accelerating both horizontally and vertically are shown in Figs. 13-17 and tables 8-14. The calibration data is presented in Fig. 13 (vertical) and Fig. 14 (horizontal). For the case of vertical acceleration in deep water, Fig. 15 shows experimental results obtained by vibration testing for comparison with theory and the agreement appears to be quite good. It may be noted that the effect of the free surface is always to decrease the added mass coefficients while the proximity of a rigid boundary has the opposite effect. All of the computer results for the sphere have been generated using 264 nodal points.

The well-known classical solution for a sphere gives an added mass coefficient of .5 for the case of a fluid of

infinite extent. Accordingly, as d becomes large, the coefficient plotted in Fig. 12 is expected to approach this closed form result but approximately a 4.0 per cent deviation is noted. This error is due to numerical inaccuracies and approximations used in the computer program.

The same kind of results are plotted in Fig. 16 as generated by the computer, the only difference being the finite depth, h = 4.0. The same general trends as in Fig. 12 are observed when the sphere is near the free surface; the rigid boundary results are greater than .5 while the free surface results are less than .5. However, as the depth is increased and the sphere approaches the bottom, the added mass coefficient increases in either case.

Theoretical and experimental results for the added mass coefficient in horizontal acceleration corresponding to a bottom mounted sphere is shown in Fig. 17. The experimental results were obtained by use of the test rig shown in Figs. 3 and 4. The sphere was mounted on the lower plate by use of a 6.0 inch strut and the sphere was adjusted to within .02 inches of the tank floor. It may be noted that the results show good agreement with theoretical results and have the same general trends as previous results except for the break off in A_{11} for the rigid boundary case as h becomes small. This reversal in trend is caused by the unwetting of the sphere occurring at values of h less than 2.0.

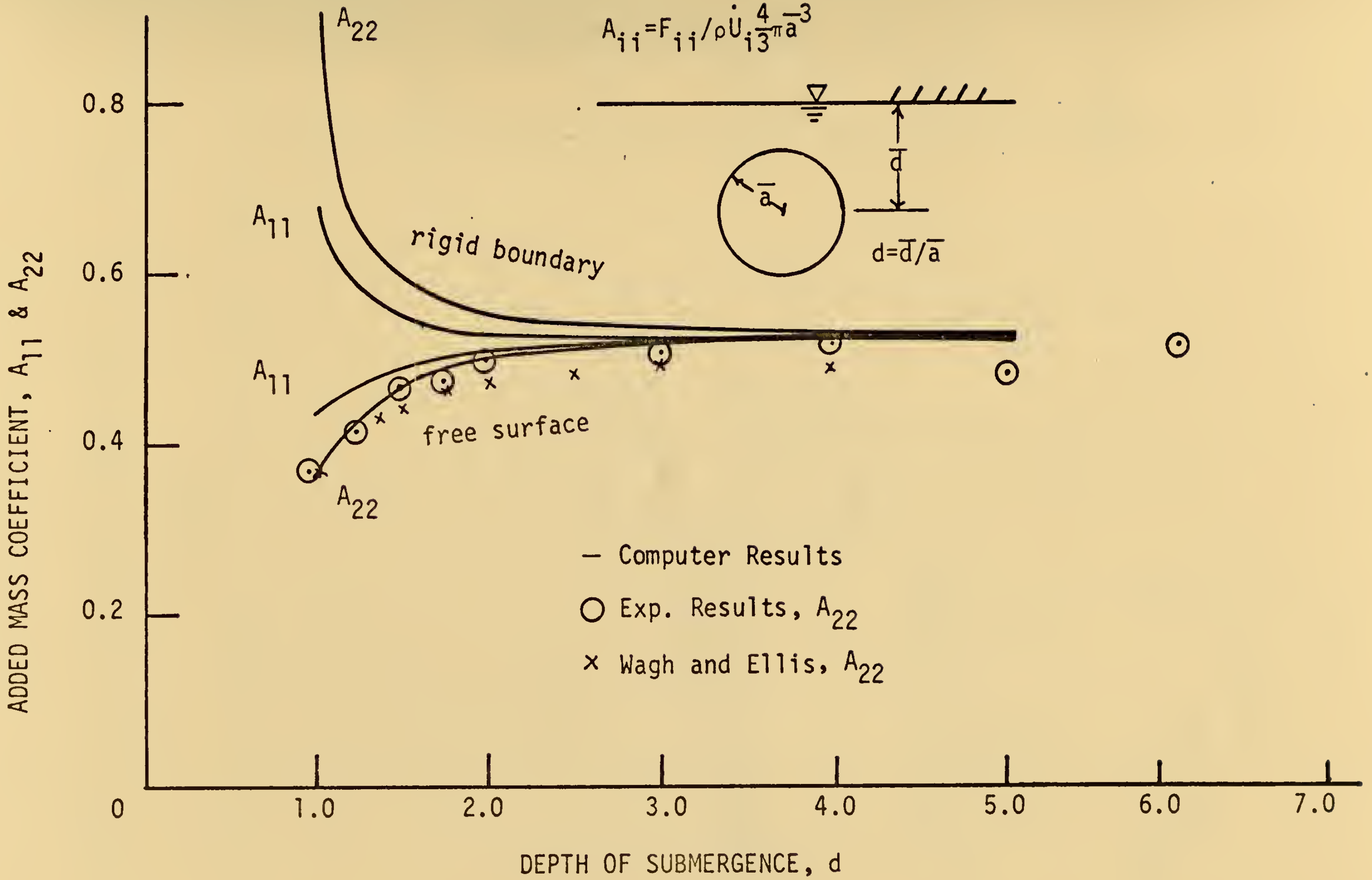

Fig. 15 - Added mass coefficient for a sphere in a fluid of infinite depth.

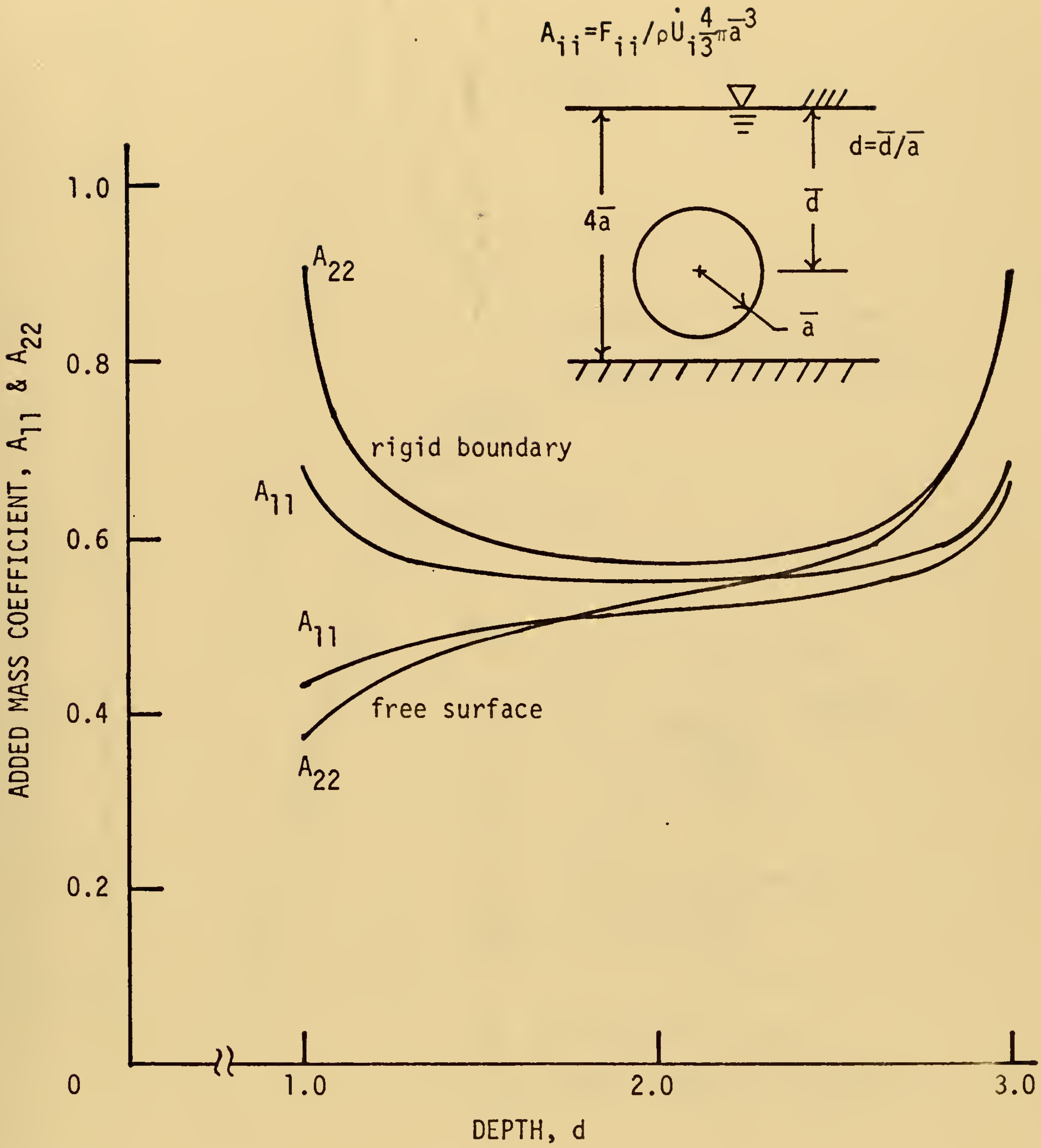

Fig. 16 - Added mass coefficient for a sphere for h = 4.0.

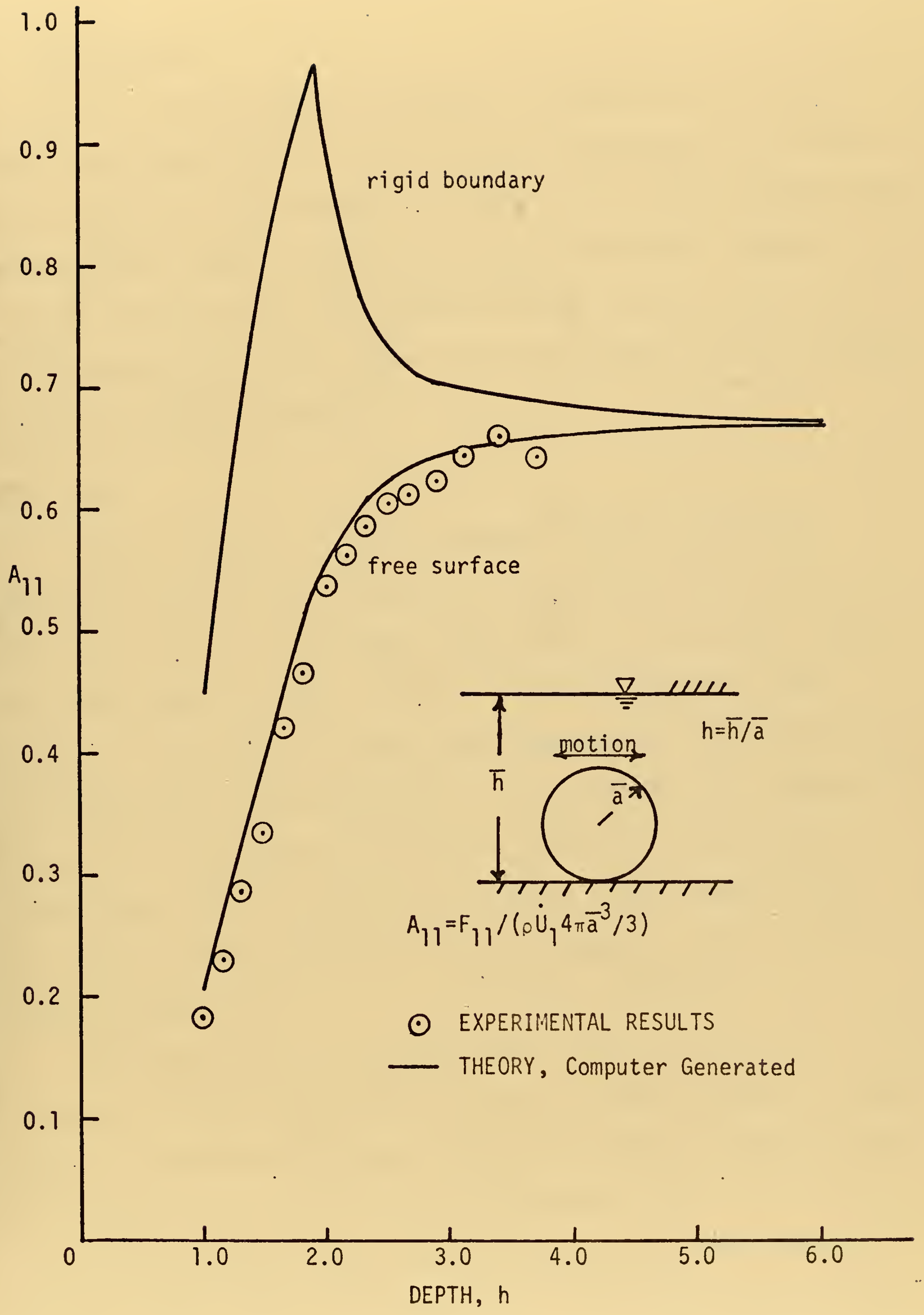

Fig. 17 - Added mass coefficient for a bottom mounted sphere.

C. HEMISPHERE

Figure 18 and Table 15 present the added mass coefficient associated with a bottom mounted hemispherical object as a function of water depth for both the rigid boundary and free surface case. The results appear somewhat similar to previous ones with the rigid boundary having the effect of increasing the added mass coefficient and the free surface having the opposite effect.

D. CONE

Conically shaped bottom mounted, surface piercing structures have been proposed for use in the Arctic on account of the ice-breaking capability of the shape. This structure shown in Fig. 19 is a conically shaped tower similar to those which have been proposed as drilling rig configurations for deployment in the Arctic. The computer results were generated using 192 effective nodal points distributed over the immersed surface. The tabular data is listed is Tables 16-18. The calibration curve is presented as Fig. 20.

The theoretical and experimental added mass coefficient (based on actual displaced volume) for the conically shaped tower is presented in Fig. 19 as a function of water depth and these results are in good agreement. The results for the rigid boundary case shows coefficients which are much greater than those corresponding to the free surface case. Moreover, for the free surface case the line of action of

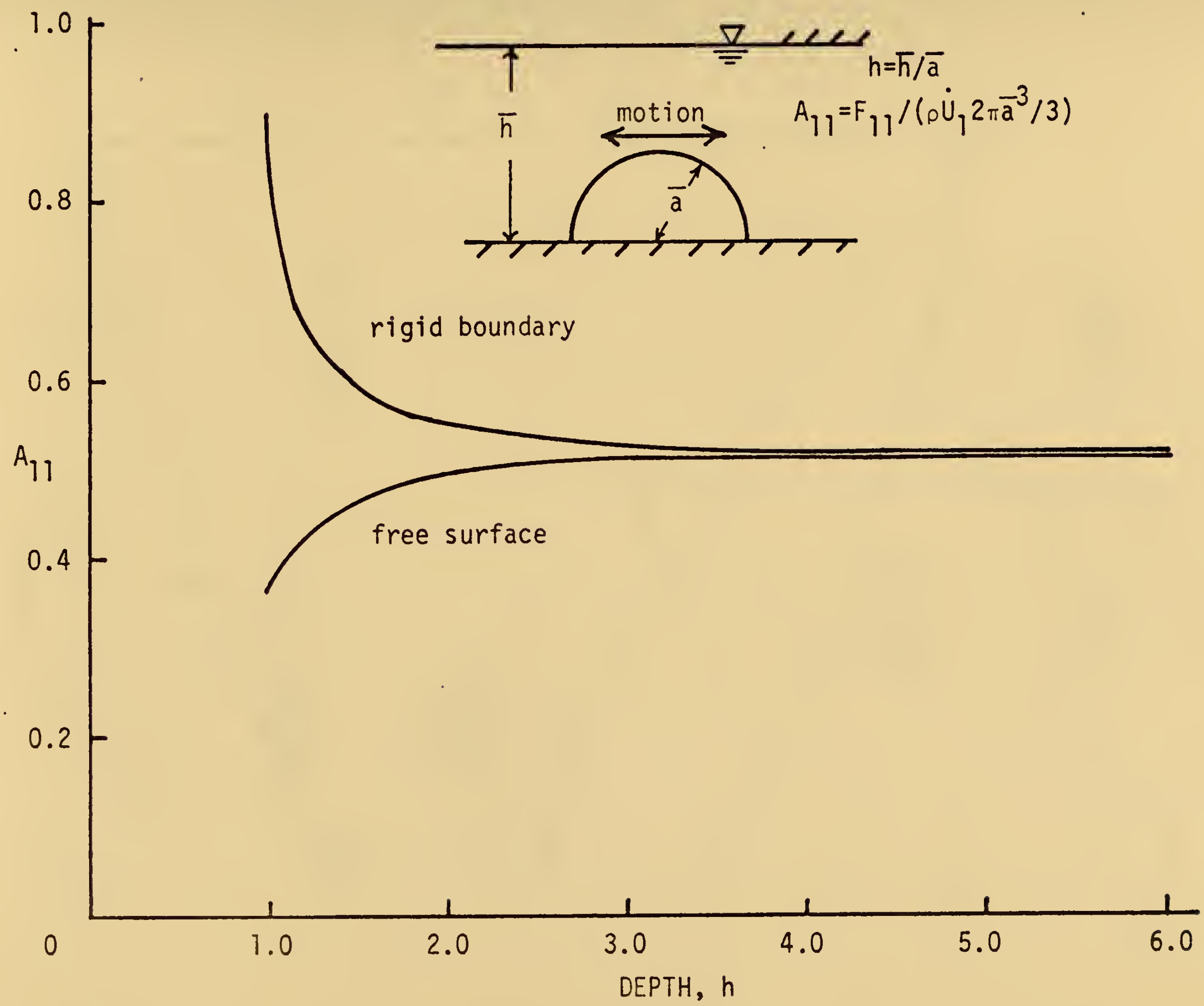

Fig. 18 - Added mass coefficient for a hemispherical vessel.

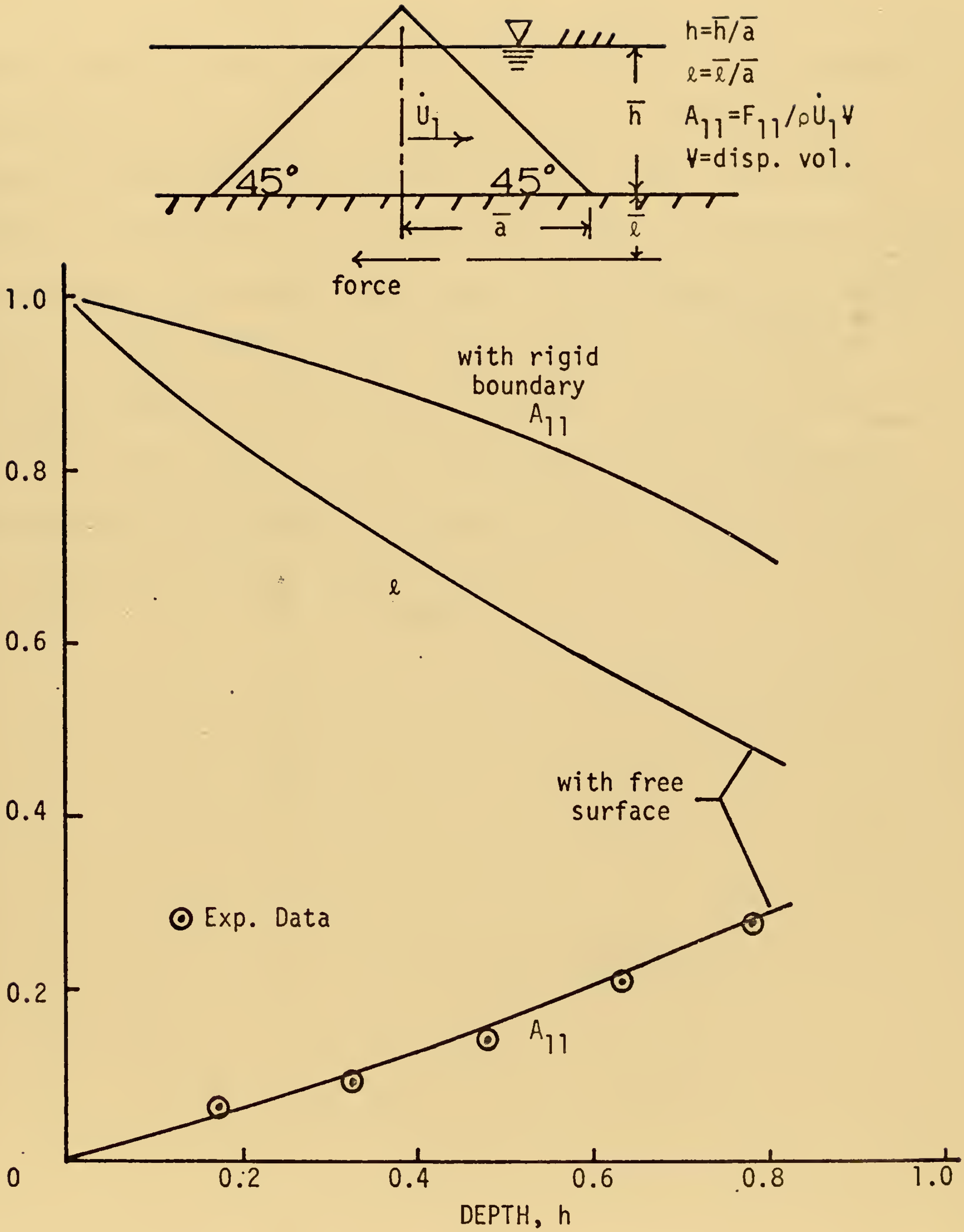

Fig. 19 - Added mass coefficient and line of action of horizontal force for a cone.

the hydrodynamic force was found to actually lie below the bottom. This rather unexpected result is caused by the fact that the pressures on the lower portion contribute to a moment opposite that induced by pressures on the upper part. In general, as the object is accelerated horizontally, positive pressures are produced on the front side while negative pressures occur on the back side. Therefore, since the pressure as well as area which contributes to a negative moment is much greater than those tending to produce a positive moment, the result is a moment tending to tip the top of the cone in the direction of the acceleration. This moment is equivalent to applying the horizontal force at a distance $\bar{\ell}$ below the bottom.

V. CONCLUSIONS

A practical numerical analysis has been developed using three dimensional sources and image sources to represent the flow produced during impulsive motion of rigid structures of arbitrary shape immersed in water in proximity to a free surface. The bottom and free surface have been taken into account and it is shown that the proximity of the free surface has a sizable effect and always tends to reduce the added mass coefficients in comparison to the rigid boundary case. The experimental results obtained by vibration testing for a sphere, cylinder, and a cone were found to agree well with the theoretical results and the results for the cylinder are in agreement with analytical results. The results are directly applicable to such practical problems as the determination of earthquake loading of rigid submerged and semi-submerged bottom mounted structures as well as the calculation of required forces to lift objects of arbitrary shape.

APPENDIX A

TABLES OF COMPUTER GENERATED DATA

TABLE 1

CYLINDER: COMPUTER GENERATED DATA (Horizontal Motion)
192 Effective Points

h	$A_{11}=F_{11}/\rho\dot{U}_1\pi\bar{a}^2\bar{h}$ Free Surface Boundary Cond.	$A_{11}=F_{11}/\rho\dot{U}_1\pi\bar{a}^2\bar{h}$ Solid Boundary Cond.	$\ell = \dfrac{A_{31}}{\bar{h}\,A_{11}}$ Free Surface Boundary Cond.
10.0	0.910	1.000	0.472
9.0	0.896	0.999	0.469
8.0	0.879	0.999	0.465
7.0	0.861	1.001	0.461
6.0	0.837	1.004	0.455
5.0	0.807	1.001	0.449
4.0	0.764	1.014	0.422
3.0	0.699	1.020	0.434
2.0	0.593	1.027	0.425
1.5	0.512	1.031	0.419
1.0	0.402	1.027	0.414
0.5	0.254	1.062	0.412

TABLE 2

CYLINDER: COMPUTER GENERATED DATA (Horizontal Motion)
120 Effective Points

h	$A_{11}=F_{11}/\rho\dot{U}_1\pi\bar{a}^2\bar{h}$ Free Surface Boundary Cond.	$A_{11}=F_{11}/\rho\dot{U}_1\pi\bar{a}^2\bar{h}$ Solid Boundary Cond.	$\ell = \frac{A_{31}}{\bar{h}\,A_{11}}$ Free Surface Boundary Cond.
10.0	0.935	1.006	0.476
9.0	0.908	1.002	0.473
8.0	0.889	1.000	0.469
7.0	0.869	1.000	0.465
6.0	0.844	1.003	0.459
5.0	0.813	1.007	0.453
4.0	0.769	1.014	0.446
3.0	0.704	1.022	0.437
2.0	0.597	1.031	0.427
1.5	0.515	1.036	0.421
1.0	0.404	1.045	0.416
0.5	0.255	1.069	0.410

TABLE 3

CYLINDER: COMPUTER GENERATED DATA (Horizontal Motion)
252 Effective Points

h	$A_{11}=F_{11}/\rho\dot{U}_1\pi\overline{a}^2\overline{h}$ Free Surface Boundary Cond.	$A_{11}=F_{11}/\rho\dot{U}_1\pi\overline{a}^2\overline{h}$ Solid Boundary Cond.	$\ell = \frac{A_{31}}{\overline{h}\ A_{11}}$ Free Surface Boundary Cond.
10.0	0.907	0.999	0.471
9.0	0.893	0.998	0.468
8.0	0.877	0.998	0.464
7.0	0.858	0.999	0.460
6.0	0.835	1.002	0.455
5.0	0.804	1.006	0.449
4.0	0.761	1.011	0.442
3.0	0.697	1.017	0.433
2.0	0.590	1.022	0.424
1.5	0.510	1.026	0.419
1.0	0.400	1.032	0.414
0.5	0.250	1.051	0.410

TABLE 6

CYLINDER: COMPUTER GENERATED DATA (Rotational Motion about vertical axis) 192 Effective Points

h	$A_{66}=M_{66}/(\rho\dot{\Omega}_3\pi\bar{a}^2\bar{h}^3)$ Free Surface Boundary Cond.	$A_{66}=M_{66}/(\rho\dot{\Omega}_3\pi\bar{a}^2\bar{h}^3)$ Solid Boundary Cond.
10.0	0.266	0.322
9.0	0.258	0.320
8.0	0.248	0.319
7.0	0.237	0.317
6.0	0.225	0.314
5.0	0.209	0.312
4.0	0.190	0.308
3.0	0.166	0.302
2.0	0.132	0.294
1.5	0.110	0.288
1.0	0.083	0.282

TABLE 7

CYLINDER: COMPUTER GENERATED DATA (Pressure Coefficients, Free Surface Boundary Condition)

$p_1 = \frac{P_1}{\rho_1 \dot{U}_1 \bar{a}}$	$d = \bar{d}/\bar{a}$	$h = \bar{h}/\bar{a}$
0.929	4.722	5.0
0.925	4.167	5.0
0.916	3.611	5.0
0.900	3.056	5.0
0.875	2.500	5.0
0.835	1.944	5.0
0.769	1.389	5.0
0.649	0.833	5.0
0.394	0.278	5.0
2.833	0.847	3.0
2.500	0.841	3.0
2.167	0.827	3.0
1.833	0.804	3.0
1.500	0.769	3.0
1.167	0.716	3.0
0.833	0.637	3.0
0.500	0.510	3.0
0.167	0.279	3.0

TABLE 7 cont.

$p_1 = \dfrac{P_1}{\rho_1 \dot{U}_1 \bar{a}}$	$d = \bar{d}/\bar{a}$	$h = \bar{h}/\bar{a}$
0.743	1.889	2.0
0.735	1.667	2.0
0.719	1.444	2.0
0.693	1.222	2.0
0.655	1.000	2.0
0.601	0.778	2.0
0.522	0.556	2.0
0.405	0.333	2.0
0.208	0.111	2.0
0.522	0.944	1.0
0.515	0.833	1.0
0.500	0.722	1.0
0.477	0.611	1.0
0.445	0.500	1.0
0.401	0.389	1.0
0.340	0.278	1.0
0.255	0.167	1.0
0.120	0.056	1.0

TABLE 8

SPHERE: COMPUTER GENERATED DATA (Infinite Fluid Depth)

d	$A_{11}=F_{11}/\rho\dot{U}_1 \frac{4}{3}\pi \bar{a}^3$ Free Surface Boundary Cond.	$A_{11}=F_{11}/\rho\dot{U}_1 \frac{4}{3}\pi \bar{a}^3$ Solid Boundary Cond.	$A_{22}=F_{22}/\rho\dot{U}_2 \frac{4}{3}\pi \bar{a}^3$ Free Surface Boundary Cond.	$A_{22}=F_{22}/\rho\dot{U}_2 \frac{4}{3}\pi \bar{a}^3$ Solid Boundary Cond.
5.0	0.516	0.518	0.521	0.524
3.0	0.513	0.520	0.515	0.530
2.0	0.504	0.520	0.498	0.548
1.8	0.500	0.534	0.489	0.558
1.6	0.493	0.542	0.475	0.574
1.4	0.482	0.555	0.454	0.603
1.2	0.463	0.580	0.419	0.660
1.1	0.450	0.603	0.394	0.721
1.0	0.432	0.671	0.363	0.901
0.5	0.190	0.222	0.292	0.453

TABLE 11

SPHERE: COMPUTER GENERATED DATA (h = 4)

d	$A_{11}=F_{11}/\rho\dot{U}_1\frac{4}{3}\pi a^3$ Free Surface Boundary Cond.	$A_{11}=F_{11}/\rho\dot{U}_1\frac{4}{3}\pi a^3$ Solid Boundary Cond.	$A_{22}=F_{22}/\rho\dot{U}_2\frac{4}{3}\pi a^3$ Free Surface Boundary Cond.	$A_{22}=F_{22}/\rho\dot{U}_2\frac{4}{3}\pi a^3$ Solid Boundary Cond.
3.0	0.663	0.682	0.898	0.904
2.9	0.595	0.613	0.717	0.725
2.7	0.556	0.576	0.620	0.632
2.5	0.538	0.559	0.578	0.595
2.3	0.526	0.551	0.554	0.578
2.0	0.514	0.547	0.529	0.570
1.8	0.507	0.549	0.513	0.573
1.6	0.498	0.555	0.495	0.585
1.4	0.485	0.566	0.470	0.610
1.2	0.465	0.590	0.433	0.665
1.1	0.451	0.613	0.407	0.725
1.0	0.433	0.682	0.375	0.904
0.5	0.190	0.225	0.300	0.880

TABLE 12

SPHERE: COMPUTER GENERATED DATA (Horizontal Motion, Bottom Mounted)

h	$A_{11}=F_{11}/(\rho\dot{U}_1 4\pi\bar{a}^3/3)$	$A_{11}=F_{11}/(\rho\dot{U}_1 4\pi\bar{a}^3/3)$
	Free Surface Boundary Cond.	Solid Boundary Cond.
6.0	0.669	0.674
5.0	0.667	0.676
4.0	0.663	0.682
3.0	0.648	0.701
2.5	0.625	0.732
2.0	0.555	0.901
1.90	0.529	0.960
1.62	0.440	0.860
1.43	0.371	0.752
1.22	0.292	0.609
1.00	0.211	0.451

TABLE 15

HEMISPHERE: COMPUTER GENERATED DATA (Horizontal Motion)

h	$A_{11}=F_{11}/(\rho\dot{U}_1 2\pi\bar{a}^3/3$ Free Surface Boundary Cond.	$A_{11}=F_{11}/(\rho\dot{U}_1 2\pi\bar{a}^3/3)$ Solid Boundary Cond.
6.0	0.516	0.518
5.0	0.515	0.519
4.0	0.514	0.520
3.0	0.510	0.526
2.5	0.505	0.533
1.7	0.481	0.567
1.4	0.455	0.610
1.2	0.421	0.674
1.0	0.366	0.901

TABLE 16

CONE: COMPUTER GENERATED DATA (Horizontal Motion)

h	$A_{11}=F_{11}/\rho\dot{U}_1\forall$ Free Surface Boundary Cond.	$A_{11}=F_{11}/\rho\dot{U}_1\forall$ Solid Boundary Cond.
6.0	0.885	0.901
4.0	0.869	0.922
3.0	0.845	0.960
2.0	0.766	1.109
1.5	0.664	1.405
1.25	0.578	1.857

---

h	ℓ Free Surface Boundary Cond.	ℓ Solid Boundary Cond.
6.0	0.336	0.336
4.0	0.338	0.335
3.0	0.339	0.333
2.0	0.348	0.324
1.5	0.370	0.305
1.25	0.394	0.281

APPENDIX B

EXPERIMENTAL DATA

TABLE 4

CYLINDER: CALIBRATION DATA (Horizontal Motion)

Cylinder (A)

Frequency (HZ)	Added Weight (lbs)
18.00	0.00
16.15	0.793
15.70	1.022
15.30	1.275
14.45	1.814
14.15	2.043
13.85	2.296
13.80	2.308
13.25	2.790
12.70	3.329
11.80	4.360
11.10	5.388

Cylinder (B)

Frequency (HZ)	Added Weight (lbs)
18.95	0.00
16.63	0.864
15.27	1.561
14.86	1.866
14.10	2.351
13.80	2.591
13.48	2.880
12.47	3.888
12.04	4.373
11.67	4.890

TABLE 5

CYLINDER: EXPERIMENTAL DATA (Horizontal Motion)

Cylinder (A)

h	Frequency (HZ)	$A_{11} = \frac{\text{Added Wt.}}{\text{Displaced Wt.}}$
5.30	12.10	0.835
4.80	12.50	0.821
4.20	13.00	0.804
3.70	13.48	0.775
3.15	14.10	0.722
2.75	14.55	0.682
2.25	15.30	0.618
2.00	15.66	0.585
1.65	16.10	0.548
1.25	16.75	0.441
0.90	17.20	0.380
0.40	17.78	0.221
0.00	18.00	0.000

Cylinder (B)

h	Frequency (HZ)	$A_{11} = \frac{\text{Added Wt.}}{\text{Displaced Wt.}}$
5.30	12.43	0.818
4.80	12.80	0.816
4.20	13.40	0.788
3.70	13.92	0.745
3.15	14.60	0.694
2.75	15.07	0.678

TABLE 9

SPHERE: CALIBRATION DATA (Vertical Motion)

Frequency (HZ)	Added Weight (lbs.)
19.8	0.0
19.0	0.3
18.6	0.5
18.3	0.7
17.5	1.0
16.7	1.3
16.4	1.5
16.0	1.7
15.4	2.0
15.1	2.3
15.0	2.5
14.6	2.7
14.4	3.0

TABLE 10

SPHERE: EXPERIMENTAL RESULTS (Vertical Motion, Infinite fluid Depth)

h	$A_{22} = \frac{\text{Added Weight}}{\text{Displaced Weight}}$
6.0	0.514
5.0	0.480
4.0	0.514
3.0	0.504
2.0	0.500
1.75	0.475
1.5	0.463
1.25	0.416
1.0	0.367

TABLE 13

SPHERE: CALIBRATION DATA (Horizontal Motion, Bottom Mounted)

Frequency (HZ)	Added Weight (lbs.)
14.65	0.379
14.35	0.592
14.00	0.828
13.95	0.864
13.65	1.077
13.40	1.313
13.00	1.625
12.75	1.873
12.25	2.390
11.85	2.875
11.45	3.397
10.75	4.405

TABLE 14

SPHERE: EXPERIMENTAL DATA (Horizontal Motion, Bottom Mounted)

h	Frequency HZ	$A_{11} = \frac{\text{added wt.}}{\text{displaced wt.}}$
3.72	12.05	0.644
3.40	12.00	0.661
3.13	12.05	0.644
2.90	12.10	0.624
2.67	12.15	0.612
2.50	12.20	0.605
2.33	12.25	0.585
2.17	12.35	0.563
2:00	12.45	0.536
1.83	12.70	0.465
1.67	12.90	0.421
1.50	13.20	0.355
1.33	13.55	0.287
1.17	13.85	0.230
1.00	14.15	0.179
0.00	15.32	0.00

TABLE 17

CONE: CALIBRATION DATA (Horizontal Motion)

Frequency (Hz)	Added Weight (lbs.)
17.61	0.418
16.89	0.631
16.50	0.867
15.53	1.352
15.11	1.664
14.62	1.912

TABLE 18

CONE: EXPERIMENTAL DATA (Horizontal Motion)

h	Frequency (Hz)	$A_{11} = \frac{\text{Added Wt.}}{\text{Displaced Wt.}}$
0.79	15.32	0.281
0.64	16.03	0.214
0.48	16.89	0.142
0.33	17.79	0.095
0.17	18.66	0.065

APPENDIX C
CALIBRATION CURVES

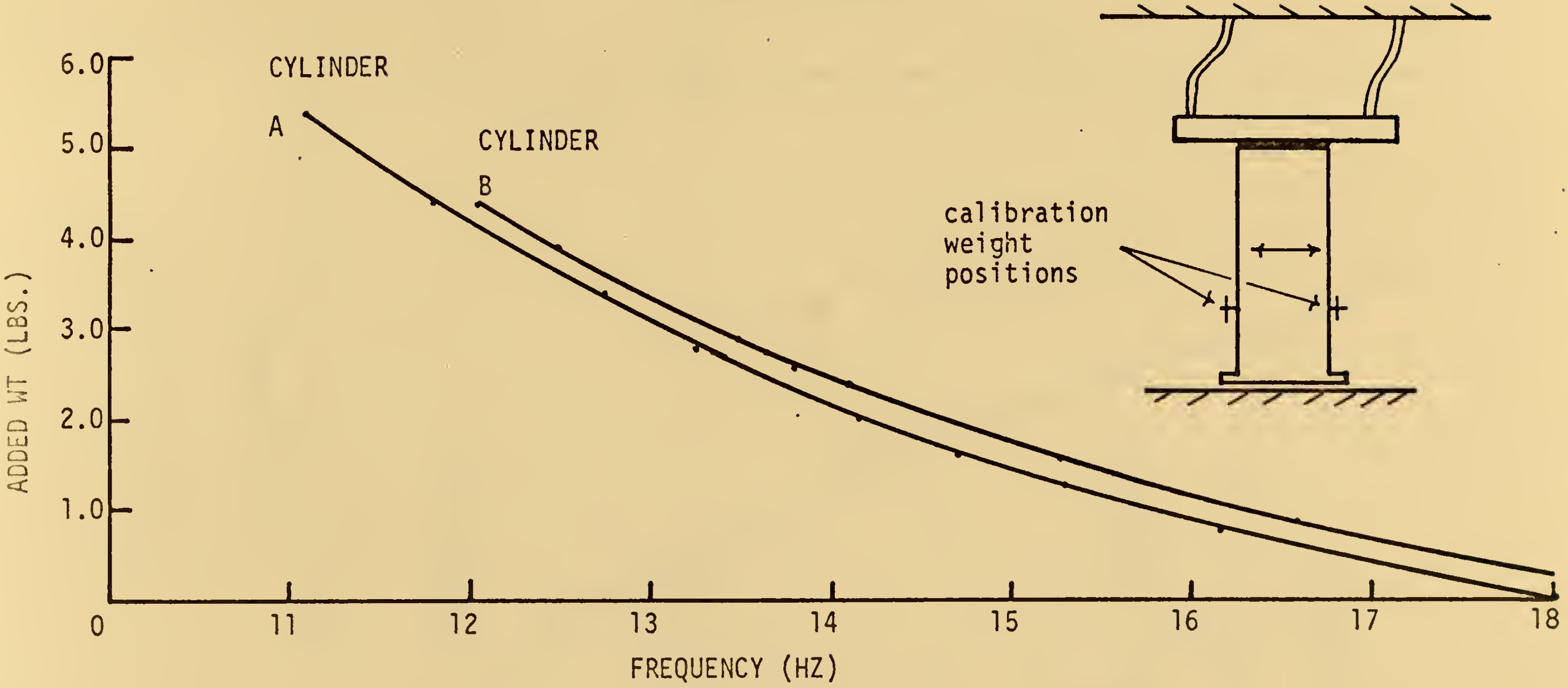

Fig. 7 - Calibration Curve (CYLINDER)

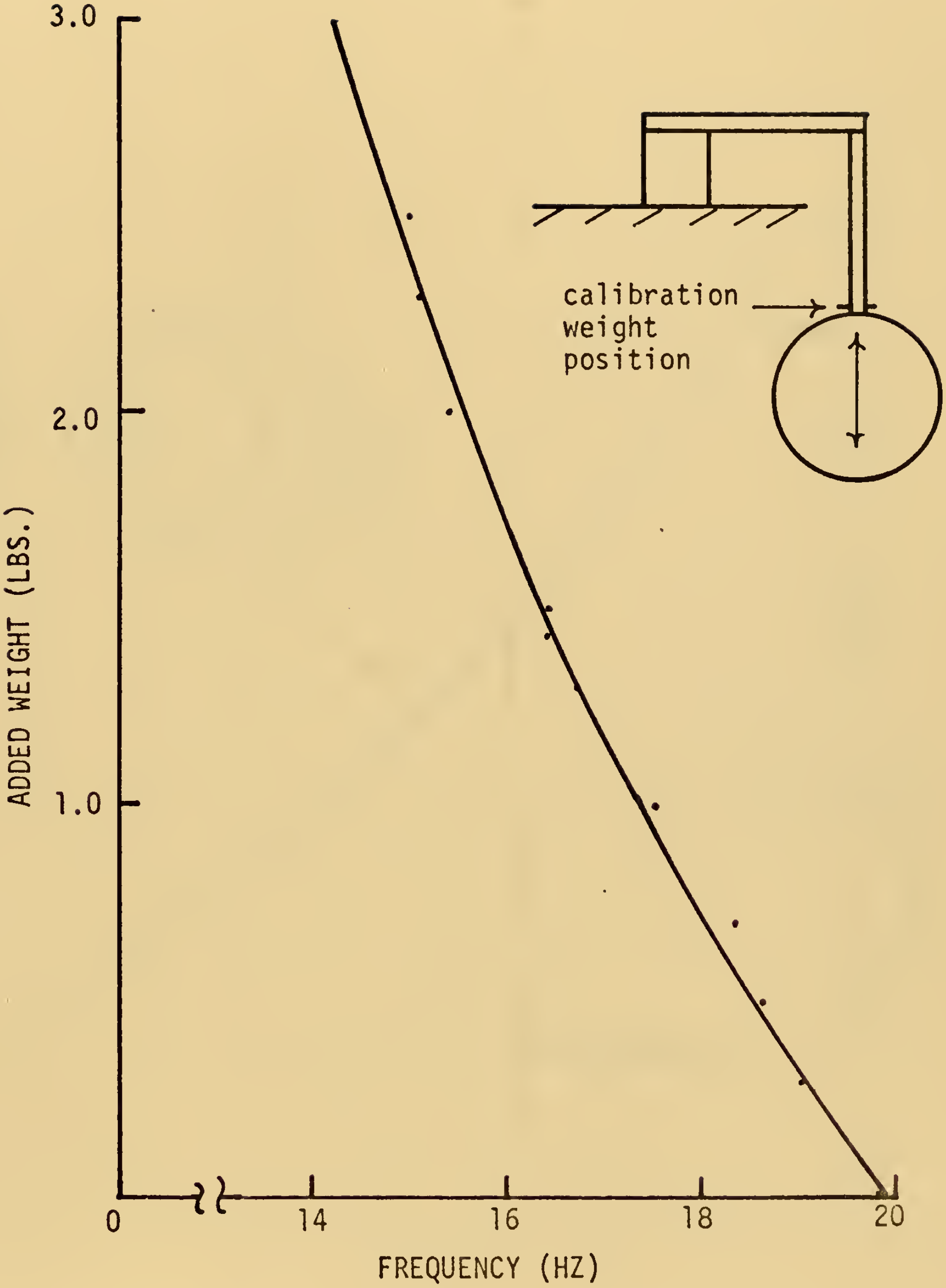

Fig. 13 - Calibration curve
(Sphere - Vertical Motion)

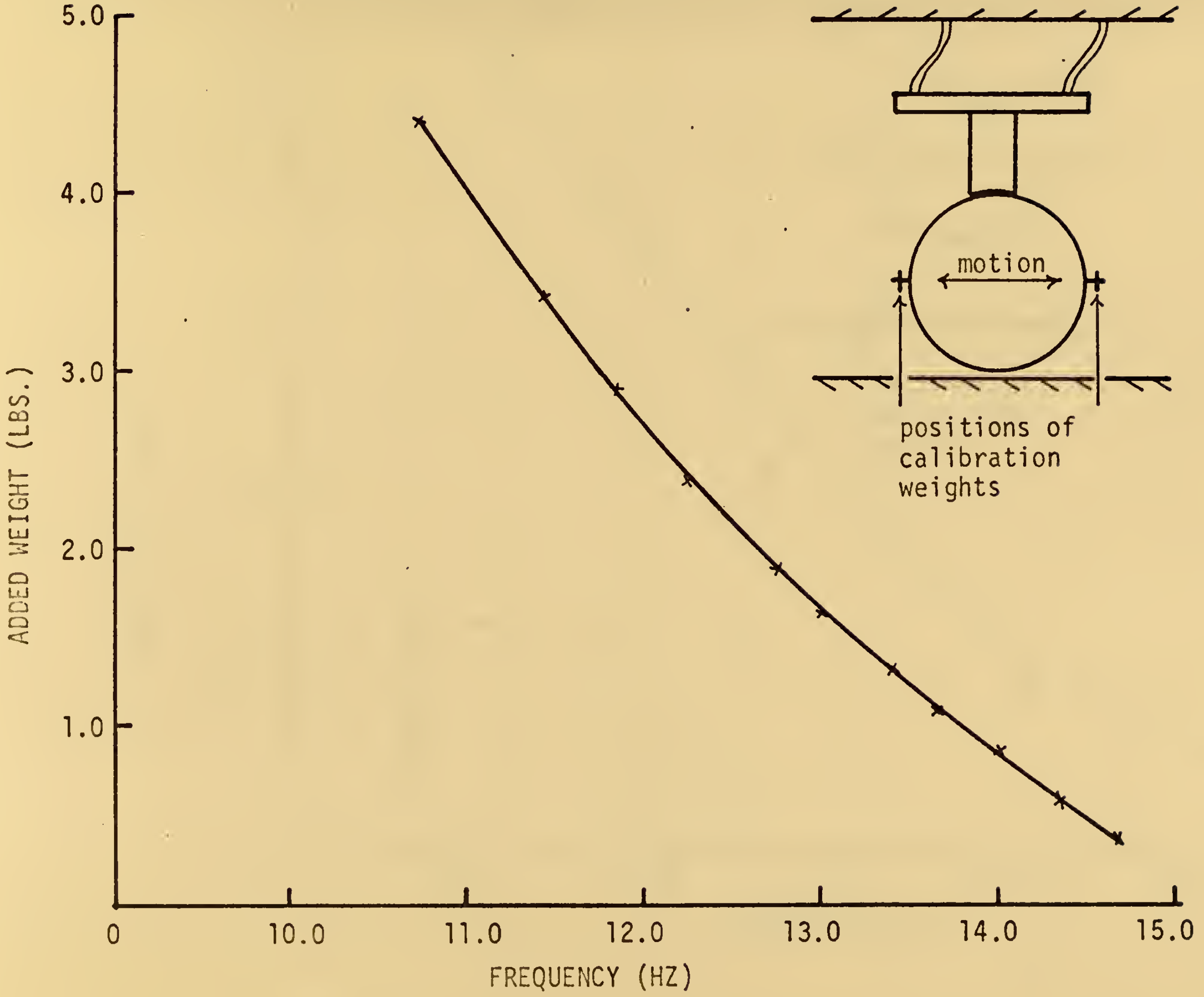

Fig. 14 - Calibration curve (Sphere - Horizontal Motion)

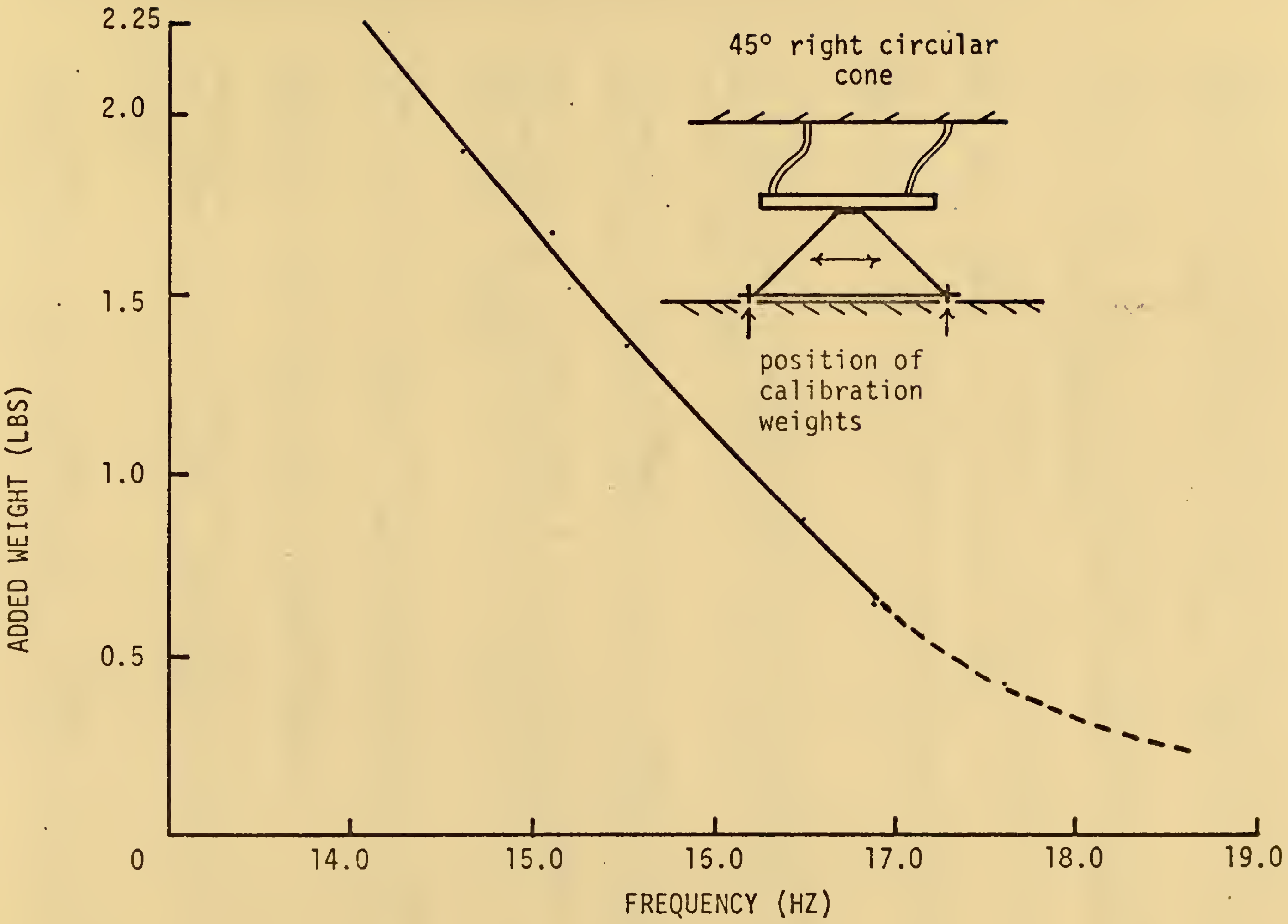

Fig. 20 - Calibration curve (Cone - Horizontal Motion)

LIST OF REFERENCES

1. Keulegan, G. H. and Carpenter, L. H.: "Forces on Cylinders and Plates in an Oscillating Fluid," J. of Research of the National Bureau of Standards, Research Paper No. 2856, v. 60, No. 5, May 1958.

2. Southerland, Jr., A.: "Mechanical Systems for Ocean Engineering," Naval Ship Systems Command Technical News, v. 39, p. 2-17, March 1972.

3. John, F.: "On the Motion of Floating Bodies II," Comm. Pure Appl. Math., v. 3, 45-101, 1950.

4. Kim, W. D.: "On the Harmonic Oscillation of a Rigid Body on a Free Surface," J. Fluid Mech., v. 21, 427-451.

5. Garrison, C. J. and Seetherama Rao, V.: "Interaction of Waves with Submerged Objects," J. Waterways, Harbors and Coastal Engineering Div., Proc. ASCE, v. 97, No. WW2, May 1971.

6. Milgram, J. H. and Halkyard, J. E.: "Wave Forces on Large Objects in the Sea," J. Ship Research, June 1971.

7. Garrison, C. J. and Chow, P. Y.: "Forces Exerted on a Submerged Oil Storage Tank by Surface Waves," J. Waterways, Harbors and Coastal Engineering Div., Proc. ASCE (in press).

8. Bowden, P. K., "Wave Interaction with Large Submerged Objects," M. S. Thesis, Naval Postgraduate School, 1971.

9. Newman, J. N.: "The Exciting Forces on Fixed Bodies in Waves," J. Ship Research, December 1962.

10. Landweber, L.: "Added Mass of Lewis Forms Oscillating in a Free Surface," Proc. Symposium on the Behavior of Ships in a Seaway, Netherlands Ship Model Basin, Sept. 1957.

11. Landweber, L. and Macagno, M.: "Added Mass of Two-Dimensional Forms Oscillating in a Force Surface," J. Ship Research, v. 1, November 1957.

12. Landweber, L. and Macagno, M.: "Added Mass of Two-Dimensional Forms by Conformal Mapping," J. Ship Research, June 1967.

13. Waugh, J. G. and Ellis, A. T.: "Fluid-Free-Surface Proximity Effects on a Sphere Vertically Accelerated from Rest," J. Hydronautics, v. 3, No. 4, October 1969.

14. Jacobsen, L. S.: "Impulsive Hydrodynamics of Fluid Inside a Cylindrical Tank and of Fluid Surrounding a Cylindrical Pier," Bulletin of the Seismological Society of America, v. 39, No. 3, 1949.

INITIAL DISTRIBUTION LIST

		No. Copies
1.	Defense Documentation Center Cameron Station Alexandria, Virginia 22314	2
2.	Library, Code 0212 Naval Postgraduate School Monterey, California 93940	2
3.	Asst Professor C. J. Garrison, Code 59 Gm Department of Mechanical Engineering Naval Postgraduate School Monterey, California 93940	3
4.	Asst Professor A. L. Schoenstadt, Code 53Zh Department of Mathematics Naval Postgraduate School Monterey, California 93940	1
5.	Asst Professor E. B. Thornton, Code 58Tm Department of Oceanography Naval Postgraduate School Monterey, California 93940	1
6.	Department of Mechanical Engineering, Code 59 Naval Postgraduate School Monterey, California 93940	1
7.	LCDR Ronald B. Berklite 854 Anthony Ave. Waynesboro, Pennsylvania 17268	2

DOCUMENT CONTROL DATA - R & D

(Security classification of title, body of abstract and indexing annotation must be entered when the overall report is classified)

1. ORIGINATING ACTIVITY *(Corporate author)* Naval Postgraduate School Monterey, California 93940	2a. REPORT SECURITY CLASSIFICATION Unclassified 2b. GROUP

3. REPORT TITLE

Added Mass of Submerged Objects of Arbitrary Shape

4. DESCRIPTIVE NOTES *(Type of report and, inclusive dates)*

Master's Thesis; September 1972

5. AUTHOR(S) *(First name, middle initial, last name)*

Ronald Betts Berklite

6. REPORT DATE	7a. TOTAL NO. OF PAGES	7b. NO. OF REFS
September 1972	83	14

8a. CONTRACT OR GRANT NO.	9a. ORIGINATOR'S REPORT NUMBER(S)
b. PROJECT NO.	
c.	9b. OTHER REPORT NO(S) *(Any other numbers that may be assigned this report)*
d.	

10. DISTRIBUTION STATEMENT

Approved for public release; distribution unlimited.

11. SUPPLEMENTARY NOTES	12. SPONSORING MILITARY ACTIVITY Naval Postgraduate School Monterey, California 93940

13. ABSTRACT

Hydrodynamic loads induced on large underwater structures by impulsive motion may be significant design factors. Such loads may be induced by earthquake excitation or may result from acceleration produced while lifting an object in the sea.

The theoretical approach to the calculation of these loads is outlined and numerical results are presented for several submerged configurations including a vertical cone, a sphere, and a vertical circular cylinder.

Numerical results for these submerged structures are presented in the form of a dimensionless load parameter or added mass coefficient. Results corresponding to a number of different water depths are presented to show the rather sizable effect of the relative water depth on the hydrodynamic force. It is shown that the effect of the free water surface is to reduce the hydrodynamic loads in comparison to the corresponding infinite depth values.

Experimental results obtained by vibration testing are presented for a submerged sphere, a cone and a vertical cylinder. These results show excellent agreement with the theoretical results.

14 KEY WORDS	LINK A		LINK B		LINK C	
	ROLE	WT	ROLE	WT	ROLE	WT
Added Mass Hydrodynamic Loads Earthquake Loads						

DD FORM 1 NOV 65 1473 (BACK)

S/N 0101-807-6821

A-31409